A critical analysis of the ^{2}H NMR data in chlorhexidine-containing model membranes

by

Hoda Talo

B.Sc., Damascus University, 2009

A THESIS SUBMITTED IN PARTIAL FULFILMENT OF
THE REQUIREMENTS FOR THE DEGREE OF

MASTER OF SCIENCE

in

The Faculty of Mathematics and Sciences

Department of Physics

BROCK UNIVERSITY

April 19, 2018

Abstract

Deuterium nuclear magnetic resonance spectroscopy was used to study the influence of chlorhexidine on the internal molecular motions of phospholipid model membranes. Mixtures of dimyristoylphosphocholine (DMPC) and chlorhexidine (CHX) were investigated at several DMPC:CHX molar ratios (1:0,10:1,3:1). Extensive numerical analysis of previously acquired data identified the differences in the temperature-dependence of the order parameters characterizing the rapid molecular motions (on the NMR scale) in both the fatty acid chains of DMPC and in the saturated methylene bridge of CHX. The results are consistent with the known localization of CHX in the membrane determined by neutron scattering [1] and confirmed by molecular dynamics simulations reported earlier [2]. The NMR results indicate that chlorhexidine undergoes different motions than those of the bulk lipids in the membrane.

The study used a Tikhonov-regularization-based numerical deconvolution technique (dePakeing) that allowed simultaneous determination of the order parameter and of the orientational distribution of domains in the powder sample, partially oriented by the external magnetic field. Both appeared to suggest an anomalous result in a narrow temperature region for the 3:1 sample, perhaps the existence of a new re-entrant phase, but this conclusion could not be made from the limited data available, and requires a further investigation.

Contents

List of Tables

List of Figures

Acknowledgements

I would like to express my sincere gratitude to my supervisor, Dr. Edward Sternin for his patience, cooperation, and guidance throughout this research. Thank you for giving me the golden opportunity to work in a great environment as Brock University and to constantly encouraging me to do the work perfectly.

I would like to offer my sincere appreciation for the learning opportunity provided to me by all of the members of the Physics Department at Brock University.

Special thanks to my colleagues and friends for all of the help, advice, and friendship throughout these years.

Many thanks to my family; especially my brother, for caring, love, and support from afar.

To my husband, I would not be who I am now without your inspiration and support. You always encouraged me to keep going and you helped me a lot to be stronger and to face all struggles, stress, and hardships. I love you so much...

To my lovely kids, thanks for being there in my life to ease the hard time with your innocent and sweet smiles, and your joyfulness. My success in this work is my gift to you, and I hope it will make up for the time that I could not spend with you. I love you.

Chapter 1

Introduction

1.1 Lipids and Membranes

Cell membranes enable the function and establish the structure of cells. Cells, the building blocks of all organisms, are all similar in their chemical composition, but differ structurally as well as in the way they replicate. The most noteworthy of these differences is the lack of nucleus in the two types of prokaryote cells (bacteria and Archean), and its presence in eukaryote cells. However, the most basic common structural feature that all cells have is the cell membrane. Membranes found in cells and viruses come in three different varieties: plasma membranes, intracellular membranes and enveloped viruses membranes. Despite the fact that each membrane performs unique tasks, there is a number of common motifs. Compartmentalization is a very important membrane motif, membrane separating one intracellular component from another and enabling control over communication between the compartments. Membranes also supply cells with energy stored in chemical and charge gradients, and provide substrates for biosynthesis and for the transport of signaling molecules. Transduction of molecular information is facilitated by membranes that transmit extracellular signals and cause an intracellular response. In addition, membranes organize and control enzyme activities which function as biochemical catalysts. Many enzymes are either membrane-bound or membrane-associated. Thus, many biological and biochemical processes couldn't be done without the cell membranes [3].

1.1.1 Membrane Historical Perspective

In 1972, Singer and Nicholson [4] amalgamated all the membrane designs that had been described earlier in the nineteenth century; Davson-Danielli and Robertson's unit models [5], into their fluid mosaic model. Early models of the membrane are depicted in Fig. 1.1. The fluid mosaic model depicts all membranes as fluid-like phospholipid bilayers in which globular molecules of integral proteins are embedded to varying degrees. Moreover, Singer and Nicholson described the globular proteins and the phospholipids to be structurally asymmetric as they are amphipathic, with a polar region in direct contact with the aqueous phase and a non-polar region embedded in the hydrophobic interior of the membrane. Based on their experimental results, several factors determine the amphipathic structure of protein: the amino acid sequence, the covalent structure, and its interactions with its molecular environment, maintaining the free energy of the system at a minimum. As discussed in the following section, the amphipathic structure of phospholipids is ensured by the hydrophilic head groups facing the water at each surface of the bilayer, and the hydrophobic tails shielded from the water in the interior of the

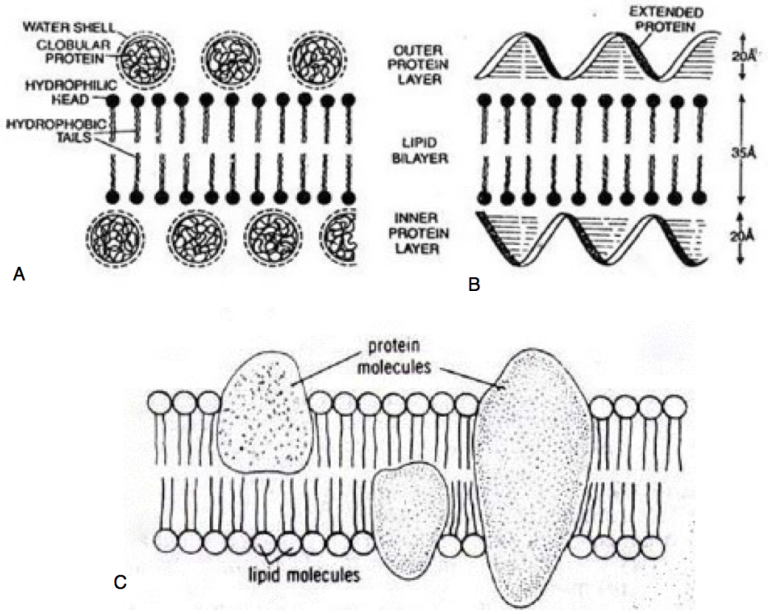

Figure 1.1: **Early models of the structure of biological membranes**: (A) the Davson Daniel model; (B) Robertson's unit membrane; (C) the fluid mosaic model proposed by Singer and Nicholson. Figure reproduced from [4].

bilayer [3].

Following the fluid mosaic model, which emphasizes the fluidity of the bulk lipid phase of the membrane, new models have been proposed which include lateral domains of varying composition and dynamic properties, and thus form transient membrane "rafts" in the bulk of the fluid bilayer. These lipid rafts are formed both in the plasma membrane and in the intracellular membrane of many cell types and they are thought to be generally thicker than the rest of the membrane [6].

The highly anisotropic and mobile environment inside the membrane requires a description in terms of position-dependent order parameters. In addition, the techniques employed in studying and measuring the membrane micro domains of different compositions, sizes, and lifetimes, have different natural time and length scales, which may require a variety of descriptors suitable for different time and length scales. A single word "fluidity" is thus a very poor descriptor and should not be used without a clarification of context.

1.1.2 Lipids self-assembly and phase transitions

Lipids are naturally occurring organic molecules that are soluble in non-polar organic solvents and insoluble in water (a polar solvent). This group of molecules includes fats, waxes, oils and phospholipids. Lipids are the main constituents of cell membranes. A typical biomembrane may contain more than 1000 species of lipids, which vary in general structure and in the length and degree of saturation of their fatty acyl chains. A few major classes of lipids found in biomembranes are glycerophospholipids (phospholipids),

sphingolipids, sterols and linear isoprenoids.

The most abundant membrane lipids are the phospholipids. They have a polar head consisting of a phosphate group and two hydrophobic fatty acid chains (they normally contain between 14 and 24 carbon atoms) joined together by a glycerol molecule. One tail can often be unsaturated (double bonds), while the other tail is saturated. The phosphate groups can be modified with simple organic molecules such as choline. Lipid molecules are amphipathic, meaning they have a hydrophilic ("water-loving") or polar end and a hydrophobic ("water-fearing") or non-polar end. The amphipathic nature of the lipids determines the way they self-aggregate when placed in a polar solvent. Fig. 1.2 illustrates several possible structures that can arise. The bilayer is only one of several possible structural arrangements, but typically it's the one that dominates at biologically-relevant temperatures, although the inverted hexagonal (H_{II}) phase has been known to play an important role in cell fusion and endo- and exo-cytosis [8]. Lipid polymorphism can be roughly characterized by the shape of the individual lipid molecules which is described by a "shape parameter" S, defined as [9]

$$S = \frac{\text{cross-sectional area of lipid headgroup} \times \text{lipid length}}{\text{lipid volume}}. \tag{1.1}$$

Lipids with a shape parameter $S = 1$ have a fairly cylindrical shape, so they tend to prefer a bilayer configuration (the lamellar phase). Lipids that are conical ($S > 1$) or wedge-shaped ($S < 1$) tend to assemble as micelles or inverted micelles, respectively [9].

The lamellar phase is a purely geometrical description; in fact, several different structural phases assemble as lamellae: L_α (lamellar liquid crystalline), also called L_d (liquid disordered); L_β (lamellar gel) or S_o ordered solid), L_c (lamellar crystalline) phase, a highly ordered form of lipid packing driven by their head group interactions, a ripple phase P_β where long molecular axes remain parallel to each other but are tilted with respect to the bilayer normal, *etc.* In addition, lipid membrane domains with high concentration of sterol molecules exhibit a different lamellar phase called liquid ordered phase (L_o) in which the membrane has a solid-like quality similar to the gel phase but with a high rate of lateral diffusion as in the liquid-disordered phase.

Phase transitions occur in the membrane environment driven by temperature changes. The highest amount of latent heat is typically release in the gel-to-liquid-crystalline transition, also referred to as the "chain-melting" transition, T_m. Lipids differ in their chain-melting temperatures depending on their compositions, *e.g.* the length of hydrocarbon chain of each lipid and the degree of saturation. Typically, lipids with longer carbon chains and fewer double bonds tend to have higher T_m. A full phase diagram of even a simple model membrane system can be quite complex, as shown in the example of a DMPC-cholesterol system of Fig. 1.3.

1.1.3 Diffusion of lipids and membrane proteins

The word "fluid" in the fluid mosaic model refers to the rapid, fluid-like, motion of lipid molecules and proteins within the 2D bilayer. Modern techniques have revealed three different motions with different rates of motion: lateral, rotational, and transverse, as

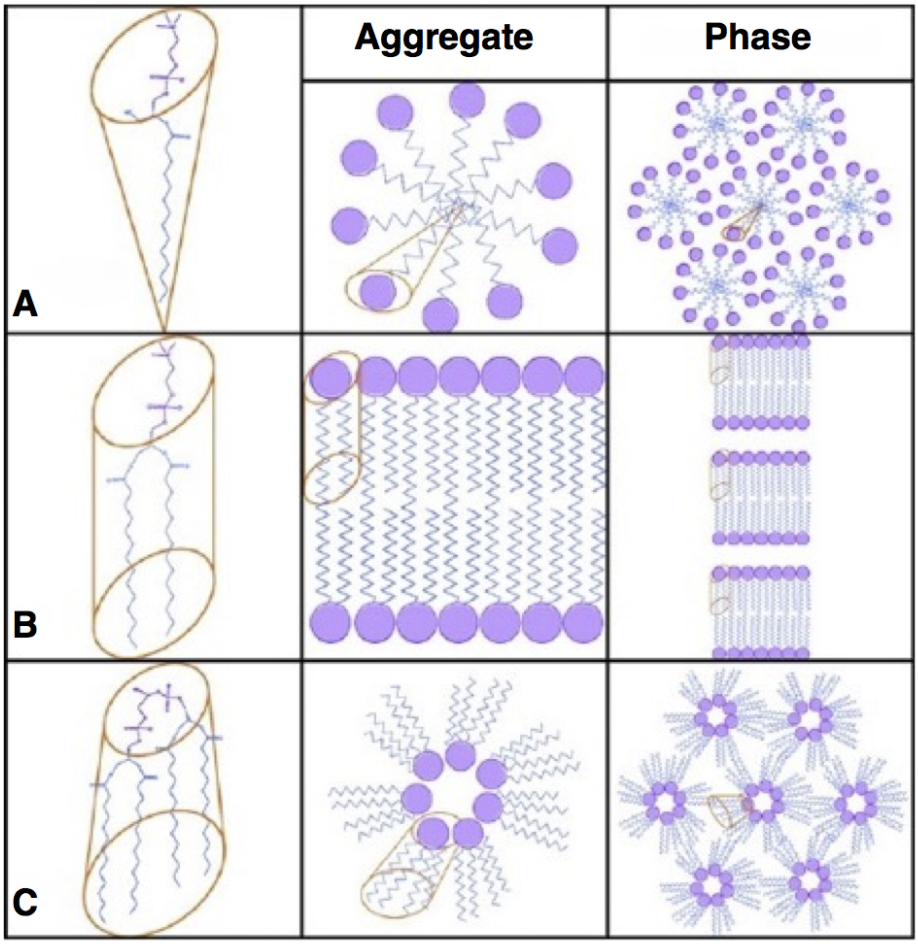

Figure 1.2: **Lipid Polymorphism is influenced by lipid shapes and aggregates**. As described in text, S is a "shape parameter" that determines the packing of individual lipid molecules: (A) for $S > 1$, lipids assemble into micelles (hexagonal H_I phase); (B) for $S = 1$ lipids form bilayers (lamellar L_α phase); (C) for $S < 1$ lipids form inverted micelles (hexagonal H_{II} phase). Figure reproduced from [7].

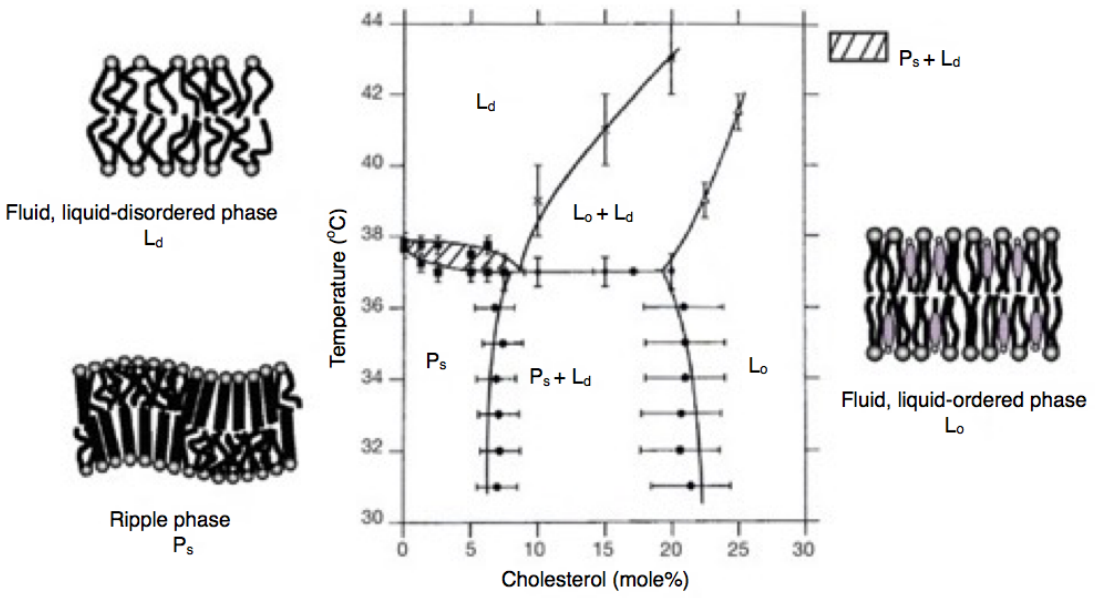

Figure 1.3: **An example of a lipid-cholesterol model membrane phase diagram.** Phase transition occurs at specific temperatures and it is influenced by cholesterol concentration. Figure reproduced from [10].

illustrated in Fig 1.4. Lateral diffusion occurs when one lipid exchanges its place with a neighbor molecule via Brownian motion; lipids travel only in the same monolayer. Rotational diffusion is the rapid reorientation of a single lipid molecule around its long axis without altering its position relative to its neighbours. Transverse diffusion or what is often called "trans-membrane flip-flop" motion is the exchange of lipid molecules between the leaflets of the bilayer [12].

Each motion has a certain characteristic time scale. The diffusion coefficient obtained by florescence recovery after photo-bleaching (FRAP), is about $1\mu m^2$/sec. While lateral diffusion in the membrane is rapid, the spontaneous flip from one leaflet to the other may occur as slowly as once in several hours. This is not surprising since a pass of lipid polar head groups through the non-polar center of the bilayer has a high free energy cost. Membrane proteins have been visualized by FRAP to be in free lateral motion (rates comparable to free diffusion of water) unless restricted by some interactions. Proteins vary noticeably in their lateral mobility. Some proteins are close in their mobility to lipids, whereas others are rather immobile, with diffusion coefficients between 10^{-5} to $10^{-1}\mu m^2$/sec.

1.2 The organization of membranes in cells

Both prokaryotic and eukaryotic cells have in common a plasma membrane that delineates the boundary of the cell and controls communication and nutrient stream into and out

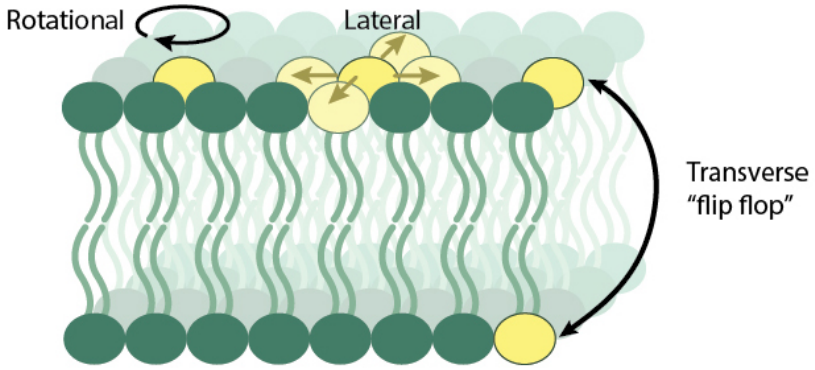

Figure 1.4: **Lipids undergo a variety of molecular motions in the bilayer**. Figure reproduced from [11].

of the cell. The schematic diagram in Fig 1.5 summarizes the current understanding of the internal organization of cell membranes [13].

In bacteria, the highly flexible cell plasma membrane is surrounded by a more rigid cell wall consisting of a thick layer of cross-linked peptidoglycan and teichoic acid. Some bacteria have an additional outer cell membrane layer, rich in lipopolysaccharides and porins (transmembrane β-barrel), which are distinct outer membrane lipid and protein components. Porins act as channels permitting passive diffusion of molecules across the outer membrane whereas lipopolysaccharides make the bilayer highly asymmetric.

The existence of the outer membrane around the cell wall prevents it from taking up Gram stain which is a staining ability some bacteria have. Therefore, bacteria with plasma membrane and cell wall structure is referred to as Gram-positive bacteria. The so-called Gram-negative bacteria do not have an outer membrane surrounding their cell wall. *E.Coli* is a much studied Gram-negative bacterium which is considered to have high resistance to antibiotics.

1.3 Chlorhexidine

An antimicrobial agent, chlorhexidine (CHX, see Fig. 1.6) is an effective drug that has been shown to have a broad spectrum of use in health care as an antiseptic and antimicrobial agent. Its power in preventing dental plaque and treating yeast infections of the mouth makes it an essential constituent to most of the oral products such as mouth wash. Chlorhexidine inactivates the majority of microorganisms such as bacteria, fungus, microfilms, and other microbial organisms because of its bacteriostatic and bactericidal mechanisms of action [15].

A substantial number of studies since the late 1940s explored CHX effectiveness and mechanism of action. Hugo and Longworth [16] demonstrated that CHX in different concentration at various pH penetrates the bacterial cells very rapidly, changing their properties and causing cell leakage. The uptake of CHX is time- and concentration-

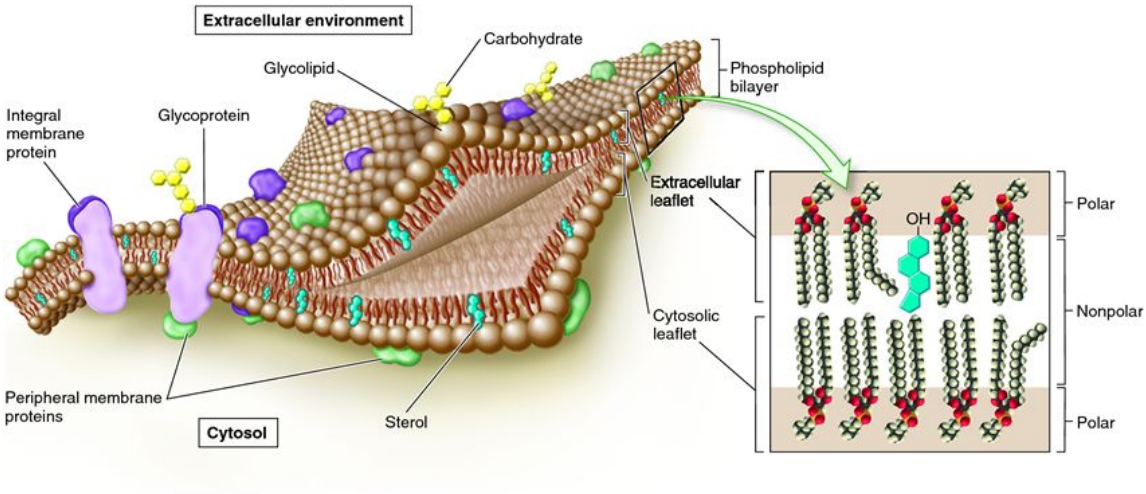

Figure 1.5: **A schematic diagram of a biological membrane**. Figure reproduced from [13].

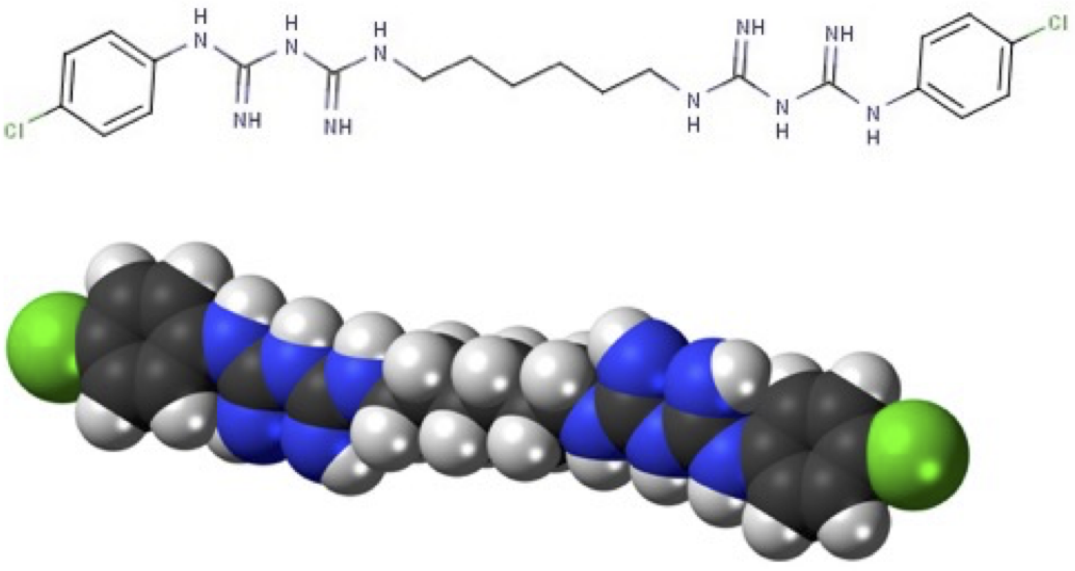

Figure 1.6: **Molecular structure of Chlorhexidine** [14]

dependent; it is bacteriostatic at low concentrations. At low concentrations, CHX is bacteriostatic; CHX has a low solubility in water and preferentially partitions into the cell membrane disrupting the cell's integrity and causing low-weight molecular components to leak out the cell. At this sublethal level, the structural changes of cytoplasmic membrane are not considerable compared to the damage caused by higher CHX concentrations [17]. Membrane damage increases at higher CHX concentration, where it forms phosphated complexes resulting in a coagulation of the cytoplasm [18]. At higher concentrations still, CHX causes irreversible cell damage [19].

CHX belongs to the bisbiguanide group and it is available as digluconate, acetate or hydrochloride salt complex, which improves its solubility. It is a symmetrical molecule with chlorophenyl rings and bis-biguanide configuration connected by a central hexamethylene bridge [20]. Similar to membrane phospholipids, the central chain represents a hydrophobic component of CHX, whereas the hydrophilic feature arises from the cationic nature of the biguanides [21]. CHX analogues with longer hydrophobic linkers could conceivably take up a trans-membrane configuration, but CHX is too short to span the typical phospholipid bilayer [22]. Instead, the CHX molecules assume a folded configuration, with both phenolic rings in close vicinity to each other, near the headgroups of the phospholipids, while its folded hydrophilic chain wedges itself into the hydrophobic interior of the membrane. This has been observed by neutron scattering, which unambiguously reports the location of the entire hexamethylene bridge to be near the headgroup-interior interface, at the depth of the glycerol backbone of the phospholipids [1] and also confirmed through molecular dynamics studies [2], as shown in Fig 1.7

Komljenovi c *et al.* (2010) have proposed that the amphiphilic nature of CHX restricts it to a wedge-like shape in a way that cleaves the lipid matrix. This proposed model is consistent with the membrane becoming more permeable in the presence of CHX, and with the observed concentration dependence. This work is the examination of whether the existing ^{2}H NMR data is consistent with this model.

It was hoped that the existing NMR data could be supplemented by the additional measurements where needed, but the scope of the data analysis that had to be done did not allow for this. It is left for a future researcher. However, all of the data collected by previous researchers in the lab [23] was critically examined. This was necessary because of the unresolved inconsistencies observed in previous work, caused both by instrumental issues and by the inconsistent thermal history of the samples during the NMR measurements.

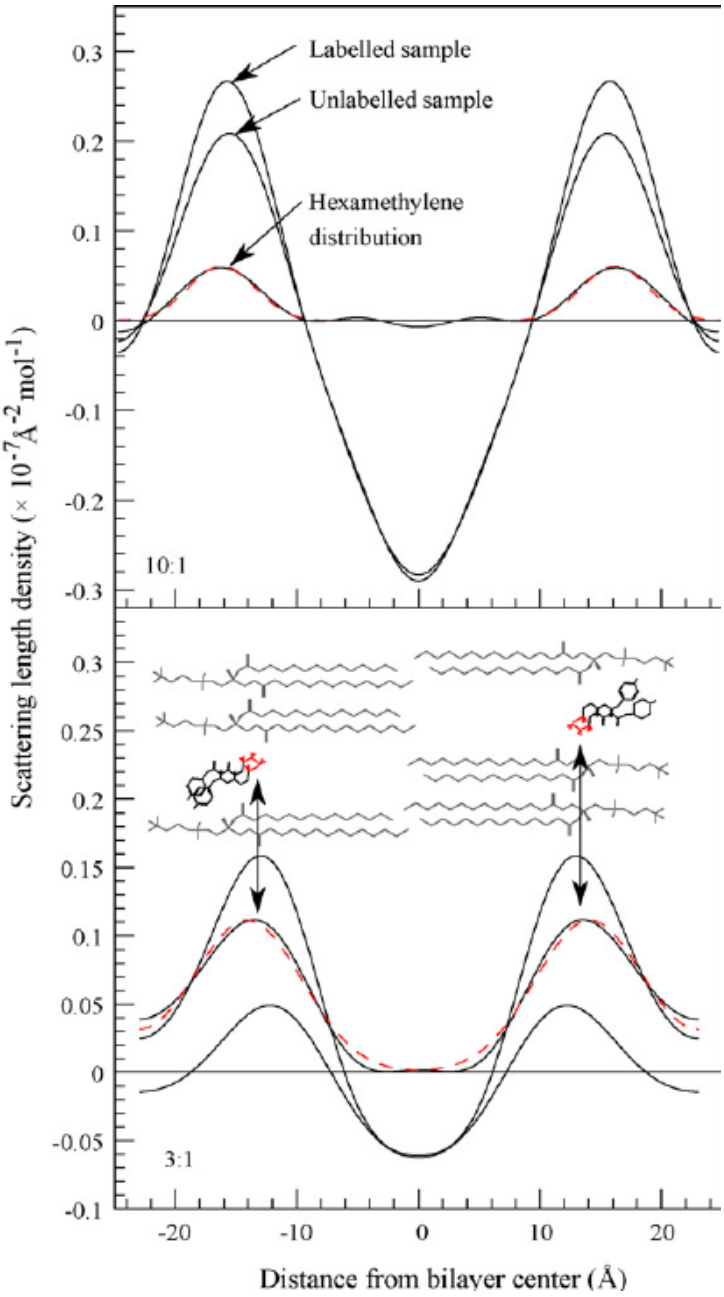

Figure 1.7: **Location of CHX in the lipid bilayer** as determined by the neutron scattering density profiles [1].

Chapter 2

^{2}H NMR in lipid membranes

Understanding the biological properties and functions of biological molecules requires detailed information about the structure, dynamics, reaction state, and chemical environment of the molecules. NMR and, in particular, solid-state ^{2}H NMR has proven itself a versatile technique capable of performing measurements over a wide range of time scales in biological systems.

Solid-state NMR spectra are much broader than the typical high-resolution NMR spectra, as the orientation-dependent interactions are not or only partially averaged by molecular motions. In systems where molecular motions occur that are faster than the time scale of the dominant interaction, partial motional averaging can reduce the observed linewidths. Biological and model membranes possess just such a property: the individual lipid molecules undergo rapid diffusion, at rates comparable to the self-diffusion of water, in the plane of the membrane, and a variety of intramolecular motions yield, on average, a nearly axially symmetric environment, with the symmetry axis along the membrane normal. The extent of this partial averaging, for axially-symmetric motions, can be described by a single order parameter S_{CD}. The designation CD refers to the direction of the gradient of the electric field associated with each C-^{2}H bond; molecular motions modulate the angle that the C-^{2}H bonds make with respect to the external magnetic field $\vec{H}_0$, and S_{CD} represents the extent of the effective time-averaged scaling of the strength of the interaction of the quadrupolar ^{2}H nucleus (spin 1) with the local electronic environment by such motions. As the molecular environment changes from site to site within a molecule, a distribution of such order parameters, or anisotropies, arises. For highly flexible molecules that make up the lipid bilayers the order parameters thus represent a measure of the nature and speed of the molecular motions. It is in this way that ^{2}H NMR of lipid membrane samples is sensitive to local molecular structure and motions which are fast on the quadrupolar interaction's time scale.

2.1 Introduction to Nuclear Magnetic Resonance

2.1.1 The classical picture

In a classical description, nuclear magnetic moments $\vec{\mu}_i = \gamma \vec{S}_i$ in an external magnetic field $\vec{H}_0$ produce a net magnetization $\vec{M} = \sum_i \vec{\mu}_i$, which precesses according to Bloch macroscopic equations of motion

$$\frac{d\vec{M}}{dt} = \vec{M} \times \vec{H}_0 \tag{2.1}$$

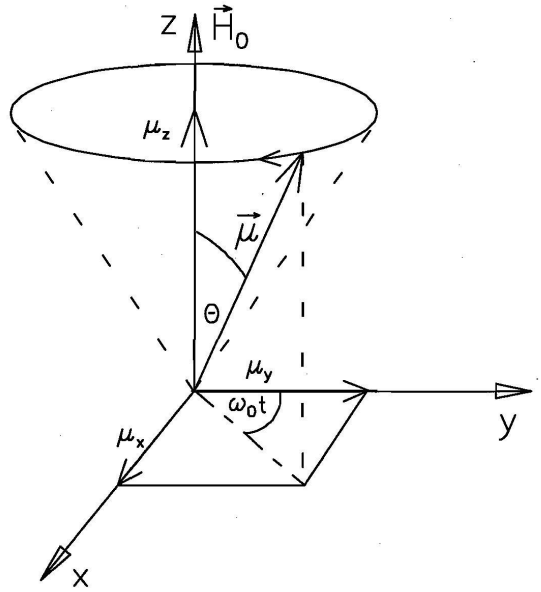

Figure 2.1: **The magnetic moment precession**. [21]

at the nuclear Larmor frequency $\omega_0 = -\gamma H_0$ where γ is the gyromagnetic ratio; a scalar property specific to each nucleus. Fig 2.1 illustrates the classical precession of the net magnetization about the field $\vec{H_0}$. In a rotating frame of reference whose z-axis is directed along $\vec{H_0}$, the transverse magnetization (*i.e.* in the xy-plane) M_0 is constant.Thus the transverse magnetization rotates around the z axis with the same angular frequency ω_0 which is the Larmor frequency of the rotating frame [24]. In a typical magnetic field of a few Tesla, most of the nuclear Larmor frequencies lie in the radio frequency range.

When a weak transverse oscillating field $\vec{H_1}(t) \propto \exp^{-i\omega_0 t}$ is applied in addition to the static field $\vec{H_0}$, this oscillating field also appears static in the rotating frame and is called the "rf field". This field causes a precession of the magnetization about the direction of the oscillating field at an angle $\theta = \gamma H_1 t_{rf}$ where t_{rf} is the time of the applied rf pulse. In NMR, the rf field that is applied long enough to rotate the magnetization from its equilibrium along the z-axis into the xy-plane is called a "90°" or a "$\pi/2$ rf pulse".

2.1.2 The quantum mechanical picture

Alternatively, NMR can be described using a quantum mechanical approach. For spin $S > \frac{1}{2}$, $2S+1$ eigenstates in an external magnetic field is described by a Hamiltonian

$$\mathcal{H} = \mathcal{H}_z + \mathcal{H}_Q \tag{2.2}$$

where $\mathcal{H}_z$ and $\mathcal{H}_Q$ represent the Zeeman and quadrupolar interactions [25], respectively. $\mathcal{H}_z$ describes the interaction of the nuclear magnetic moment with the magnetic field H_0 and is given by

$$\mathcal{H}_z = -\gamma\hbar\hat{S}_z H_0 \tag{2.3}$$

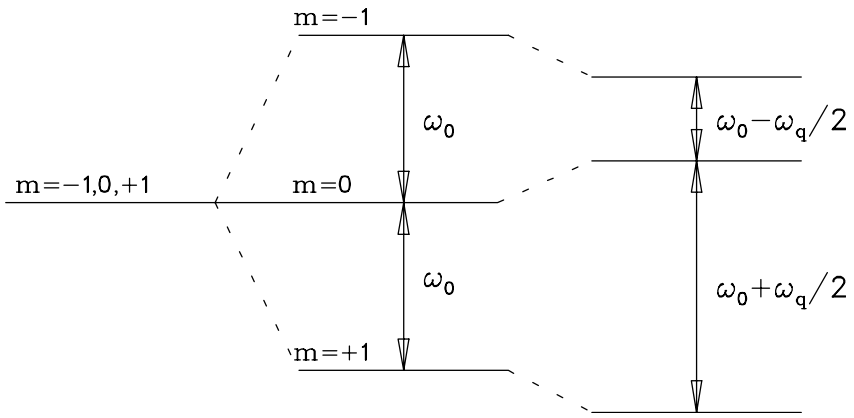

Figure 2.2: Zeeman and quadrupolar splitting

where $\hat{S}_z$ is the z-component of the spin operator $\hat{S}$ and H_0 is taken to be along the z-axis. The energy levels associated with the Zeeman splitting in an external magnetic field are separated by $\hbar\omega_0 = h\nu$ as shown in Fig. 2.2.

The probability distribution of the populations of the Zeeman energy levels at thermal equilibrium is determined by the Boltzmann factor (the ratio of probabilities for states i and j)

$$\frac{N_i}{N_j} = e^{(\varepsilon_j - \varepsilon_i)/k_B T} \tag{2.4}$$

At a given temperature, the distribution shows that the states with lower energy ε_i will always have a higher probability of being occupied than the states with higher energy ε_j.

The interactions between the quadrupolar moment eQ of the ^{2}H nucleus and the electric field gradients eq causes a slight shift of the Zeeman energy levels. This shift in energy levels increases with greater quadrupolar moments and stronger EFGs, see Fig 2.2. The EFG of the CD bond is due to the distribution of the electric charges, and can be expressed in terms of a traceless, symmetric second rank tensor V_{ij}. This tensor has 5 independent components which can be reduced by a coordinate transformation into two independent components in the principal axis system [26].

In Cartesian coordinates these two components are defined as ($V_{zz} = eq$) and $\eta \equiv (V_{xx} - V_{yy})/V_{zz}$ where η is known as the quadrupole asymmetry parameter. The quadrupolar interactions are then described by the Hamiltonian as follows

$$\mathcal{H}_q = \frac{e^2 qQ}{4S(2S-1)\hbar}\left[3\hat{S}_z^{\,2} - \hat{S}^2 + \eta\left(\hat{S}_x^{\,2} - \hat{S}_y^{\,2}\right)\right] \tag{2.5}$$

For an axially-symmetric EFG, $V_{xx} = V_{yy}$ and thus $\eta = 0$. So, the Hamiltonian can be written as

$$\mathcal{H}_q = \frac{e^2 qQ}{4S(2S-1)\hbar}\left(3\hat{S}_z^{\,2} - 2\right) \tag{2.6}$$

the term $\frac{e^2qQ}{4S(2S-1)\hbar}$ is called the quadrupolar frequency ω_q and has the form $\frac{3e^2qQ}{4\hbar}$ for the

deuterium nucleus of $S = 1$. Using the the quadrupolar term, the Hamiltonian becomes

$$\mathcal{H}_q = \frac{\omega_q}{3}\left(3\hat{S_z}^2 - 2\right) \tag{2.7}$$

the quadrupolar frequency has approximately the value of $\omega_q \approx 2\pi \times 167$ kHz for a C-D bond in a saturated hydrocarbon chain.

In order for the EFG tensor not to coincide with laboratory reference frame, a transformation from the EFG tensor principal axes to the laboratory reference frame can be made using Wigner rotation matrix $\mathcal{D}_{m'm}(\alpha\beta\gamma)$ [26]. The angles (α, β, γ) are the Euler angles defining the transformation and specifying the orientation of the principal-axes reference frame of the EFG tensor in the lab frame. The quadrupolar Hamiltonian after the transformation has the form

$$\mathcal{H}_q = \frac{e^2qQ}{4S(2S-1)\hbar}\left[3\hat{S_z}^2 - \hat{S}^2\right]\left[(3\cos^2\beta - 1) + \eta\sin^2\beta\cos 2\alpha\right] \tag{2.8}$$

which in turn leads us to the quadrupolar splitting in the laboratory frame of reference

$$\Delta\omega_q = 2\pi\Delta\nu = \omega_q\left[(3\cos^2\beta - 1) + \eta\sin^2\beta\cos 2\alpha\right] \tag{2.9}$$

Assuming that the EFG tensor is axially symmetric about the CD bond direction ($\eta = 0$), the observed quadrupolar splitting depends only on β

$$\Delta\omega_q = \frac{\omega_q}{2}\left[(3\cos^2\beta - 1)\right] \tag{2.10}$$

where β defines the angle between the CD bond and the direction of the external magnetic field H_0.

2.2 The order parameter

In deuterium NMR, the order parameter is a direct measurement of the efficiency of motions modulating and time-averaging the quadrupolar interactions $\Delta\omega_q$. This time-averaged ($\langle\rangle$) arises since the molecular motions modulate the angle $\beta(t)$. These motions are fast on the quadrupolar interactions time scale ($\Delta\nu_q \sim 127$kHz, and ${\tau_c}^{-1} <\sim 10^{-4}s$) and thus, they appear as a motional narrowing of the signal. However, multiple inequivalent locations within a molecule are not averaged out, they are instead seen as a superposition of multiple time-averaged signals.

It is convenient to describe the transformation from the EFG principal axes' frame to the lab frame in two steps. First, we transform into the molecular reference frame associated with the axis of symmetry of the (rapid) reorientational motions $\vec{d}$. The order parameter S_{CD} in the molecular reference frame given by

$$S_{CD} = \frac{1}{2}\left\langle(3\cos^2\beta' - 1) + \eta\sin^2\beta'\cos 2\alpha'\right\rangle \tag{2.11}$$

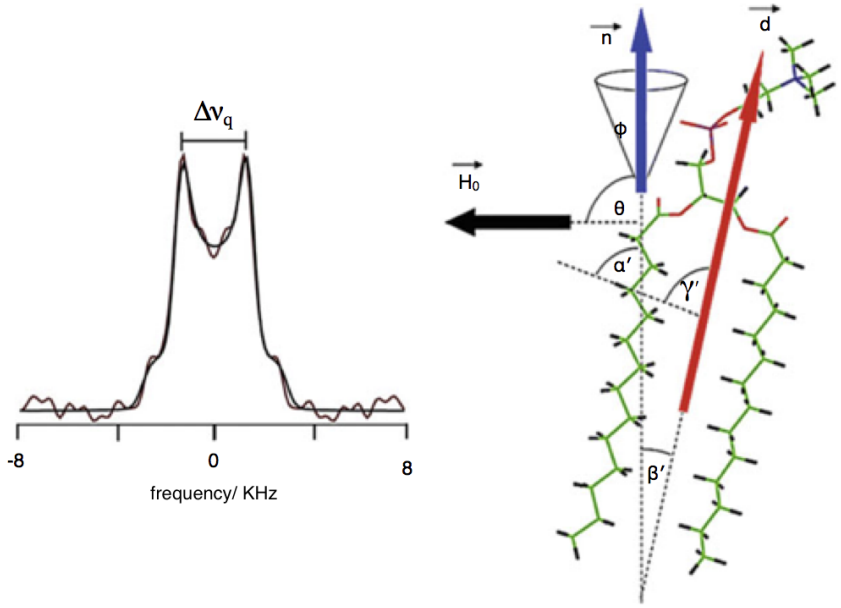

Figure 2.3: **Representation of the order Parameter via Euler angles**. A typical deuterium NMR spectrum (left) for a single C-D bond on an acyl chain of a phospholipid in the membrane bilayers. The quadrupole splitting ($\Delta\nu_q$) can be used to give information about local order of the lipid chain; the order parameter, S_{CD} on the right. The reorientations of the C-D bond vector with respect to the molecular axis $\vec{d}$ are characterized by the time-dependent angles α', β', and γ'. See the text for more details (adapted from [27]).

where α' and β' are the Euler angles that describe the transformation from the EFG frame associated with the C-D bond into the frame associated with the symmetry axis of the intramolecular motions (Fig. 2.3). When the molecular motions over which the average is calculated are fully axially-symmetric ($\eta = 0$), the latter equation of S_{CD} reduces to

$$S_{CD} = \frac{1}{2}\left\langle (3\cos^2\beta' - 1)\right\rangle \tag{2.12}$$

The second transformation, into the lab frame, is simplified by the fact that the molecular axis $\vec{d}$ is further rapidly averaged by lateral diffusion onto the membrane normal $\vec{n}$, while the fluctuations of the membrane normal with respect to the external magnetic field are typically much slower than the NMR time scale and do not average out. As seen in Fig. 2.3, θ and ϕ are the Euler angles specifying, respectively, the angle between the normal of the bilayer $\vec{n}$ and the external magnetic field, and the angle of the fluctuation of the bilayer normal in a cone shape around $\vec{n}$. Therefore, the observed quadrupolar splitting becomes

$$\Delta\omega_q = \omega_q(3\cos^2\theta - 1)S_{CD} \tag{2.13}$$

The quadrupolar splitting here depends only on θ but not on ϕ due to the axial symmetry of the fast motions.

The value of order parameter S is in the range of $0 \leq |S| \leq 1$, where $S = 1$ corresponds to a perfectly oriented system such as crystals while $S = 0$ denotes fully isotropic disordered chains (as in liquid NMR). So, in general, the smaller the value of the order parameter the greater the extent of the fast motions. Therefore, valuable information on the reorientational dynamics and the alignment of phospholipid molecules in a sample can be gained from the determination of the distribution of the order parameters.

The deuterium NMR spectra for deuterated lipid chains comprise of an overlap from all individual carbon positions, thus the distribution of order parameter profile $S_{CD}(n)$ as a function of n is needed. Here n indicates the carbon position along the fatty acid chain. $S_{CD}(n)$ decreases as the carbon number n increases, *i.e.* as the distance from the glycerol backbone grows, giving rise to a characteristic order parameter profile [8].

De-Paking [28] is a numerical deconvolution technique that can be used to obtain individual values of $\Delta\omega_q$.

2.3 The distribution functions

Phospholipid molecules of a bilayer membrane in the liquid crystalline (L_α) phase undergo a rapid, axially symmetrical reorientational motion about the bilayer normal. Thus, it is more convenient to separate the effect of the motion on the observed quadrupolar splitting by writing

$$\omega(x, \theta) = x\frac{3\cos^2\theta - 1}{2} = xP_2(\cos\theta) \tag{2.14}$$

where $x = \omega_q S_{CD}$ is the anisotropy parameter and $P_2(\cos\theta)$ describes how this anisotropy contributes to the observed spectrum, as the angle θ between the axis of symmetry of the motion and the external magnetic field changes.

In general, the experimentally observed powder spectrum $S(\omega)$ is a result of the contributions of all anisotropy parameters x represented by an anisotropy probability distribution function $g(x)$, but also from all different orientations of the different powder domains represented by the orientational probability distribution $p(\theta)$. The two descriptions are equivalent:

$$\begin{aligned} S(\omega) &= \int g(x)\left[p(\theta)\frac{\partial\theta}{\partial\omega}\right]dx \\ &= \int p(\theta)\left[g(x)\frac{\partial x}{\partial\omega}\right]d\theta \end{aligned} \tag{2.15}$$

More explicitly, $g(x)$-weighted superposition of lineshape functions, one for each anisotropy x, whereas the orientational distribution function $p(\theta)$ weighs the superposition of spectra from domains of single symmetry axis of motions. For an oriented sample, the orientation distribution function becomes $p(\theta) = \delta(\theta)$ while for a random uniform powder distribution $p(\theta) \propto \sin\theta$. If, instead, $g(x)$ is known, $p(\theta)$ can be determined. If $p(\theta)$ is known, $g(x)$ can be extracted from the powder spectrum, as is exactly the case of "de-Pake-ing" [29]

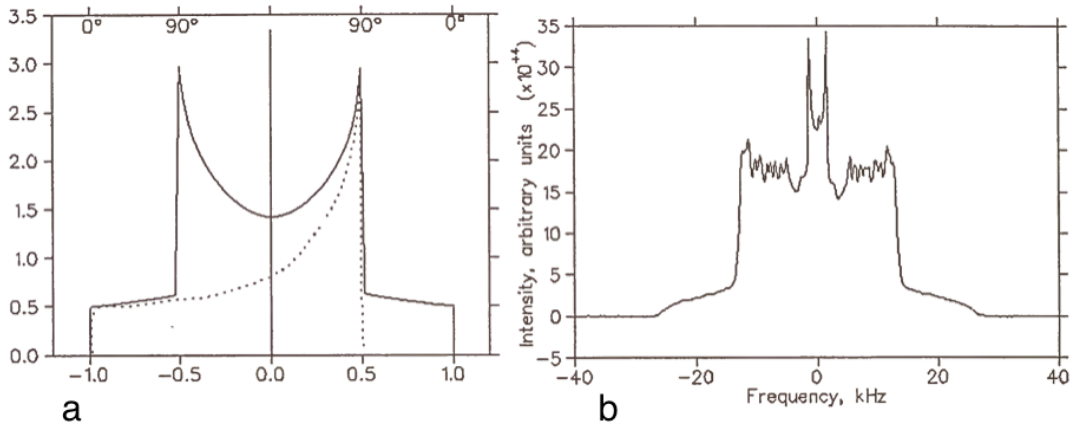

Figure 2.4: **Pake doublets and powder spectra**: (a) Powder pattern of a single isolated spin-1 system; (b) an experimental powder spectrum of a DMPC-d54.

2.4 The powder spectra and "De-Pake-ing"

The spectrum produced from a powder sample consists of a superposition of many individual quadrupolar doublets, called pake doublets or Pake pattern after G.E. Pake [30]. Each one corresponds to a particular orientation θ in the given sample and is made up of two peaks separated by a distance equal to the quadrupolar splitting $\delta\omega_q$. For an isotropic sample (random orientation), the sharp peaks indicate that the CD bonds are oriented at 90° whereas the shoulders are at 0° fig 2.4(a). "De-Pake-ing" is a numerical procedure [31, 32] of extracting both $g(x)$ and sometimes also a limited number of parameters that characterize $p(\theta)$ from the powder spectrum [33]. Many strategies have been employed to analyze experimental spectra under the conditions of partial magnetic ordering in a high external magnetic field. The Tikhonov regularization technique is one of the techniques that can be used to obtain both distribution functions simultaneously [33]. For the case of dePakeing, Eq. 2.16 can be written as

$$S(\omega) = \int g(x)C(x,\omega)dx \tag{2.16}$$

where $C(x,\omega)$ can be identified as the kernel function

$$C(x,\omega) = \begin{cases} p(\theta)\frac{\partial\theta}{\partial\omega}\,, & \text{for } -\frac{\pi}{2} < \omega \leq x \\ 0\,, & \text{otherwise} \end{cases} \tag{2.17}$$

and where

$$p(\theta)\frac{\partial\theta}{\partial\omega} = -\frac{p[\theta(x,\omega)]}{[2(x-\omega)(x+2\omega)]^{1/2}}. \tag{2.18}$$

Thus, knowing $p(\theta)$ completely determines $C(x,\omega)$ which in turn can provide the distribution function $g(x)$. However, one can only obtain an approximate pseudo-inverse $\tilde{g}(x)$, as in general, obtaining true $g(x)$ is a mathematically ill-posed problem. In fact, Eq. 2.16

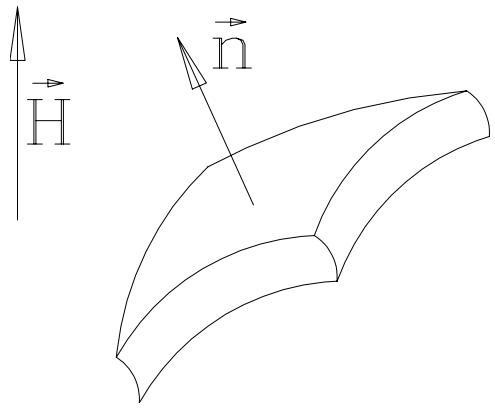

Figure 2.5: **A schematic of a bilayer domain in an external magnetic field $\vec{H}$:** $\vec{n}$ is the bilayer normal. Fig. is reproduced from [35]

is a so-called Fredholm integral equation of the first kind and is a well-known example of an ill-posed problem. The calculation of the pseudo-inverse $\tilde{g}(x)$ is also affected by the presence of experimental noise in $S(\omega)$. In this case the discrete set of experimentally collected data can be described in the following form

$$S_j^{\sigma} = S_j + \sigma_j \tag{2.19}$$

where S_j is the "exact data"; $j = 1....m$, while σ_j is the random noise that affects S_j.

For a random orientational distribution of powder samples, $p(\theta) \propto \sin\theta$, but if magnetic ordering occurs in the membrane systems this assumption does not hold [34].

2.5 $p(\theta)$ of a partially ordered system

Magnetic susceptibility of phospholipid bilayer is anisotropic, and it is given by

$$\Delta\chi = \chi_{\parallel} - \chi_{\perp} < 0\,. \tag{2.20}$$

When phospholipid bilayer is placed in a high magnetic field $\vec{H}$ used in NMR spectroscopy, a magnetic moment is induced, which in turn interacts with the field $\vec{H}$ resulting in a torque described by

$$\vec{\tau} = \Delta\chi\, A\, d\, (\vec{H}\cdot\vec{n})\, (\vec{H}\times\vec{n}) \tag{2.21}$$

where A is the area of the bilayer, d is its thickness, and $\vec{n}$ is the bilayer normal. This torque orients the bilayer preferentially so that $\vec{n} \perp \vec{H}$ is favored, see Fig. 2.5 . Thus, because of the partial magnetic ordering in the biological and model membranes, the effect of the high magnetic field on the bilayer domain orientations can not be negligible and it must be taken into account.

To deal with magnetically partially ordered systems, a method which has been established by [34] was applied. This method describes the magnetic ordering effect by a one-parameter function $p_{\kappa}(\theta)$ that describes systematic deviations from the random case of $p(\theta) \propto \sin\theta$. The parameter κ represents the degree of magnetic distortion and its

exact meaning varies depending on the model function. Several different model functions have been used to minimize the misfit $\Phi(\kappa)$ as illustrated in Fig. 2.6 ,noisy datat undertaking where the results from the following one-parameter models are compared:

Ellipsoidal model corresponds to a continuous deformation of a spherical liposome, and the orientational distribution function of this model is given by

$$p_E(\theta) \propto \sin\theta \times \left[1 - (1 - \kappa_{_E}) \cos^2\theta\right]^{-2} \tag{2.22}$$

where κ_E has the physical meaning of the square of the ratio of the long and short semi-axes of the ellipsoid or rotation. Different values of κ_E describe different possible orientations of the ellipsoid; for example $\kappa_E > 1$ is an ellipsoid with the long axis parallel to the external magnetic field. When $\kappa = 1$, the orientational distribution reduces to the case of spherical symmetry.

Legendre model represents the most general approach to describing orientational distributions, restricted in this case to a single term in the expansion in Legendre polynomials:

$$p_L(\theta) \propto \sin\theta \times \sum_{i=1}^{\infty} A_i \, P_i(\cos\theta) \approx (1 + \kappa_{_L} \cos^2\theta) \tag{2.23}$$

where $\kappa_L = 1$ corresponds to the random (spherical) orientation distribution.

Boltzmann model describes a completely uncorrelated orientation of adjacent domains within a membrane, where the probability of finding a domain of a certain orientation is given by the Boltzmann factor associated with the (orientation-dependent) energy of interaction between this domain and the magnetic field:

$$p_B(\theta) \propto \sin\theta \times \exp\left[\kappa_{_B} \cos^2\theta\right] \tag{2.24}$$

Here, $\kappa_B = 0$ corresponds to the random (spherical) orientation distribution, while $|\kappa_B| \gg 1$ corresponds to a high degree of magnetic alignment.

As Fig. 2.6 illustrates, all models can successfully characterize a mild degree of magnetic alignment typical of model membrane systems. While it is essential to take this into account for a precise determination of $g(x)$, the exact nature of the model used to optimize $p(\theta)$ is not important. For consistency, only the results of dePakeing using the ellipsoidal model are reported in this work.

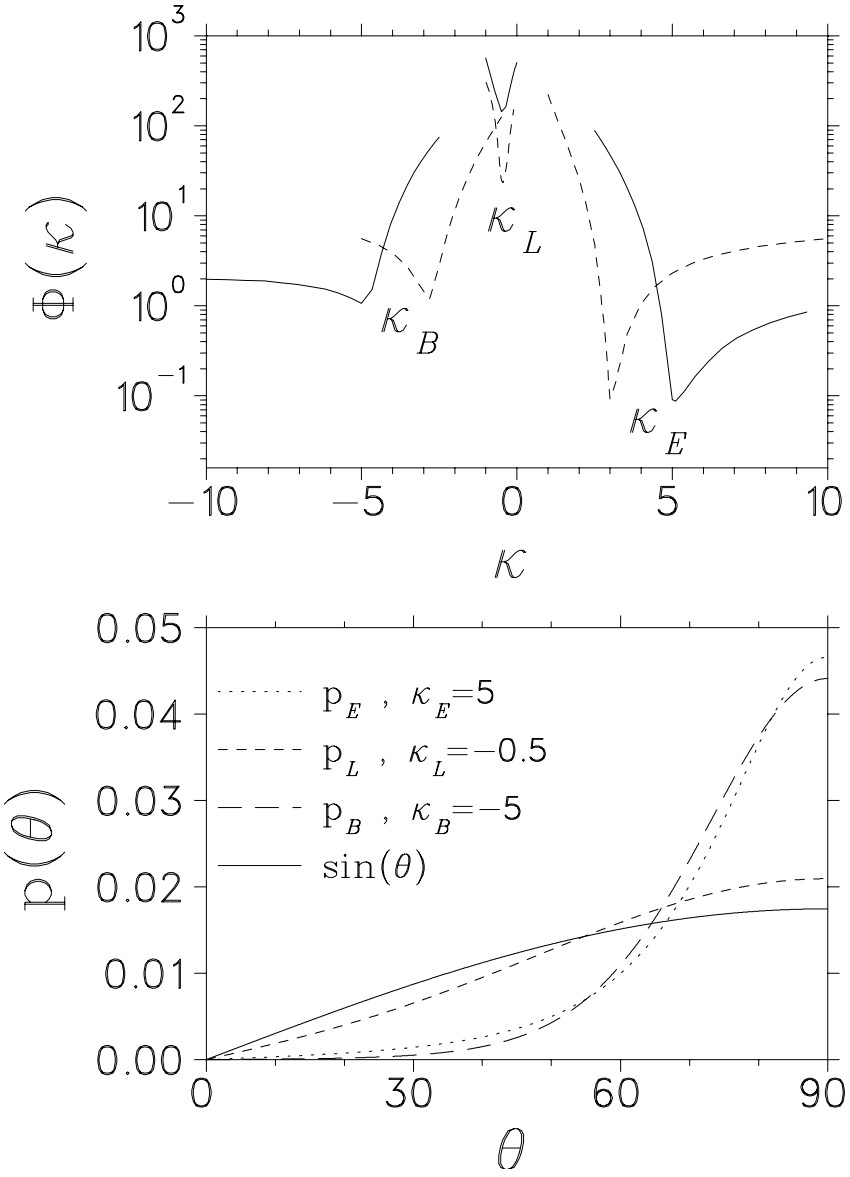

Figure 2.6: (Top) The misfit $\Phi(\kappa)$ as a function of κ. (Bottom) The three models of $p(\theta)$ as functions of the three minima of κ determined in the top plot. Fig. is reproduced from [34]

Chapter 3

Materials and Methods

3.1 Sample Preparation

Model membranes in this study consisted of pure 1,2-dimyristoyl-d_{54}-sn-glycero-3-phosphocholine (DMPC) and its analog per-deuterated (d_{54}-DMPC) lipids with various concentrations of 1,1-hexamethylene-bis[5-(4-chlorophenyl)biguanide] (Chlorhexidine, or CHX). Molar ratios of 10:1, 6:1, and 3:1 were prepared for d_{54}-DMPC:CHX and DMPC:CHX-d_8. A pure d_{54}-DMPC sample was used as a reference. The samples had been prepared by previous co-workers and the collected data was re-analyzed in this study to account for the discrepancies and inconsistencies in data processing discovered since.

DMPC was purchased from Avanti Polar Lipids (Alabastar, AL, USA) and used without further purification. Chlorhexidine digluconate solution and Chlorhexidine dihydrochloride were purchased from Sigma-Aldrich (St.Louis, MO, USA) and have also been used without further purification. A synthesis of deuterated chlorhexidine hydrochloride has been reported previously [36]. Deuterium-depleted water was purchased from Cambridge Isotope Laboratories (Andover, MA, USA), while HEPES buffer was purchased from Sigma-Aldrich (St. Louis, Mo, USA).

All samples were prepared following the same standard protocol. Powder DMPC (or d_{54}-DMPC) was dried for several hours under reduced pressure prior to use. Every sample typically consisted of about 35 mg of dry lipid to which a desired amount of a 20% stock solution of (protonated or deuterated, as required) chlorhexidine hydrochloride in deuterium-depleted water was added by volume (micro-syringe), to achieve the desired molar ratio of lipid:CHX. To maintain a consistent water-to-lipid ratio of 30:70, deuterium-depleted water was then added to the sample by a micro-syringe. Throughout, the total mass was monitored with an analytical balance. All samples were prepared in snap-closure polyethylene containers and were prepared and sealed under nitrogen atmosphere ($[O_2] < 2\%$).

Several cycles of freezing in a liquid nitrogen bath followed by thawing in a warm (65°C) water bath were performed to ensure adequate mixing; all achieved uniform semi-translucent appearance. After that, the samples were left to equilibrate at (4°C) at least overnight (8-10hrs) and up to several days before NMR spectra were collected.

3.2 NMR spectroscopy

NMR spectra were collected using a broad-band solid-state spectrometer described previously [37], in a 7.0-T superconducting magnet (Oxford Instruments) using a home-built inductively-coupled probe. ^{2}H NMR experiments were performed at a Larmor frequency

of 46.06 MHz.

The temperature of the sample was controlled by an airflow temperature controller and maintained for each experiment within ±0.2°C. After each change in temperature, the sample was equilibrated for 20 minutes and the coil tuning monitored and adjusted as necessary. The absolute error of the reported temperature was ±0.5°C. The repeat time between was set at 600 ms for the spectra acquisitions. The dwell time was set at 2μs between successive data points acquired by the digitizer, and 200-kHz Butterworth low-pass analog filters were used on the analog signals prior to digitization.

3.3 Spectral moments

The method of moments was applied to the NMR spectra to monitor the average order changes as a function of temperature for each sample. The quantitative analysis of the spectral moments M_n was based on calculating the second moment M_2 using the following

$$M_n(\omega) = \frac{1}{M_0} \int_{\omega_0-\omega_M}^{\omega_0+\omega_M} (\omega - \omega_0)^n S(\omega)\, d\omega \tag{3.1}$$

Here, $M_0 = \int S(\omega) d(\omega)$ is the area under the spectrum $S(\omega)$, centered at the Larmor frequency ω_0, $S(\omega)$ is the intensity of the ^2H-NMR spectrum, and M_n is its nth moment. The limits ($\pm\omega_M$) of the integral are chosen to be large enough to include all of the spectral intensity, as indicated by the levelling off of the calculated moments as a function of ω_M. All odd moments should vanish for a symmetric spectrum. Thus, the second moment is an appropriate measure of the average spectral width. Also, the thermodynamic changes occurring in the sample can be detected by the calculation of the second moment as a function of temperature.

3.4 Thin-layer chromatography (TLC)

Samples that were expected to be used in experiments in the research were tested for purity prior to use by the TLC technique. TLC is a common chromatography technique used widely to separate mixtures, determine their purity and identify their constituent compounds. This method is based on the use of a sheet of glass, plastic, or aluminum foil, which is coated with a thin layer of adsorbent material, usually silica gel, aluminum oxide, or cellulose (blotter paper) which represent the solid phase. The mobile phase is represented by a solvent such as acetone, methanol, distilled water and it is chosen according to the properties of the components in the substance. When a small amount of a compound or mixture is applied to the plate, a solvent or solvent mixture is drawn up the plate via capillary action. Different analytes ascend the TLC plate at different rates, so separation of the components is achieved [38].

Pre-coated silica gel plates with a layer thickness of 250 μm (Partisil K6, 5×20 cm, 60-Å average pore size) was obtained from Whatman (Sigma Aldrich). The solvent mixture used was chloroform:methanol:distilled water in 130:50:8 ratio. Iodine crystals were used

for staining purposes. Ascending chromatography was performed in a conventional TLC chamber.

Each TLC plate was prepared by marking a horizontal line across the TLC plate approximately 1.5cm from its bottom. A small mount of each membrane sample was placed on the line using a micropipette and allowed to dry. If necessary, repeated drop applications were used, drying completely between applications. Details of the steps and procedures can be found in [39]. After the plates were placed in the TLC chamber with solvent level well below the marked line and the chamber sealed, the solution rose up the plate for 15 to 45 minutes, and the position of the developed solvents was marked directly after the plate was removed from the developing chamber.

Two ways were used to visualize the compounds: by shining ultraviolet light on the plate, or by allowing the plate to stand for a few minutes in a closed container in which the atmosphere is saturated with iodine vapour. Digital scanning of the exposed plates proved more reliable than marking out the plate with pencil and measuring the distances with a ruler. An example of a developed TLC plate is shown in Fig. 3.1.

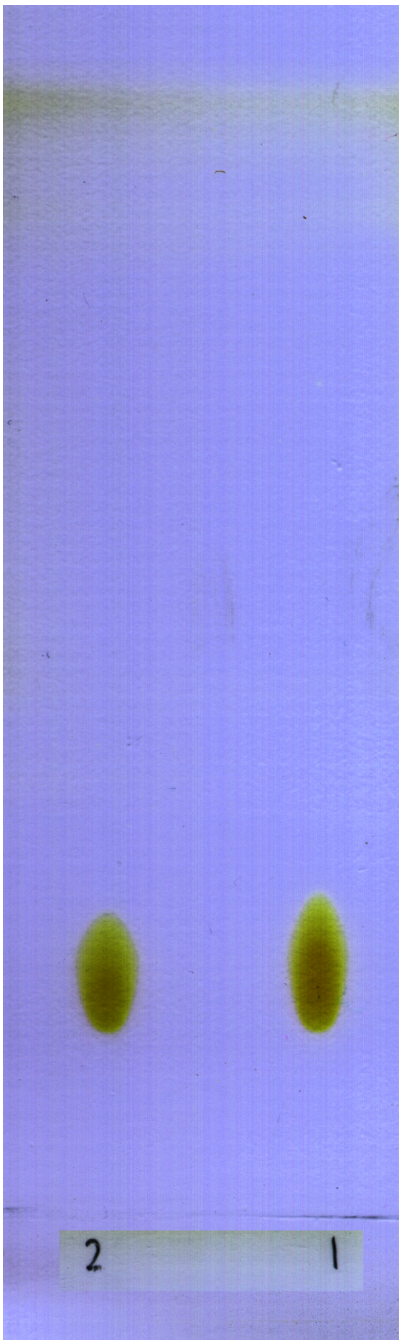

Figure 3.1: **TLC of a DMPC sample**: (1) is a powder sample of DMPC dissolved in 150μm chloroform for a concentration of 40 mg/ml, and (2) is a post-NMR sample of DMPC+water. Absence of intermediate spots indicates that the sample maintained its integrity throughout the NMR experiments.

Chapter 4

Experimental Results

4.1 Pure DMPC model membranes

^{2}H NMR spectra of the pure d_{54}-DMPC:water sample are shown in Fig. 4.1. They are in good qualitative agreement with those reported in the literature [26]. In our work careful attention to the thermal history of the sample was paid, since the earlier attempts at analysis produced inconsistent results. Here, after the sample is prepared and equilibrated at 4°C, the NMR data is collected in a series of monotonically increasing temperatures. After reaching the highest temperature of 65°, the temperature is stepped back down and NMR spectra are collected at the same temperature values. We refer to these data sets as "first heating" and "first cooling" cycles. A data set that is consistent for the same temperature values in both heating and cooling sides of the data set can be thought to be reliably reproducible. This impression is further confirmed by plotting the second moments of the spectra through the heating and cooling process, as shown in Fig. 4.2 A small thermal hysteresis is observed, but it is well within the known ±0.5°C precision of maintaining the temperature of the sample in the probe for all temperatures above $T_m = 20$°C. There is a slight discrepancy in the gel phase, but this is not surprising as the lateral diffusion, which acts as the strong macroscopic equilibration mechanism, is significantly slower in the gel phase.

The dePaked spectra of Fig. 4.1 were extracted by the regularization dePaking algorithm for the ellipsoidal orientational model at the minimum of misfit function $\Phi(\kappa)$ [34], and are shown in Fig. 4.3. The two central peaks of the spectra of Fig. 4.1 and Fig. 4.3 represent the CH_3 group of the DMPC chains while the rest of the individual peaks corresponds to the CH_2 groups. As discussed earlier, each of these peaks represents the time average over the rapid molecular motions of each CH_2 and CH_3 groups of the bilayer.

The spectra demonstrate a characteristic narrowing with increasing temperature. This is an indication of the increasingly faster motions of lipid molecules at higher temperatures. Transition from the gel crystalline phase to liquid crystalline phase occurs at 20° in both heating and cooling processes (dePaked spectra not shown) of the sample as presented in Fig. 4.3. In the liquid crystalline phase, the DMPC chains are very flexible, which means that various molecular motions are more effective in reducing the spectral widths via motional averaging. Otherwise the nature of the spectral distributions remain the same, with a "plateau" region represented by several carbon positions near the headgroup which are very similar in the extent of their motional narrowing, followed by a rapid increase in the amount of motions available further down the chain. A large number of apparent peaks is likely a byproduct of a slight inequivalence of the two deuterated chains.

The reported values of κ_E correspond to a mildly elongated ellipsoidal shapes, with a

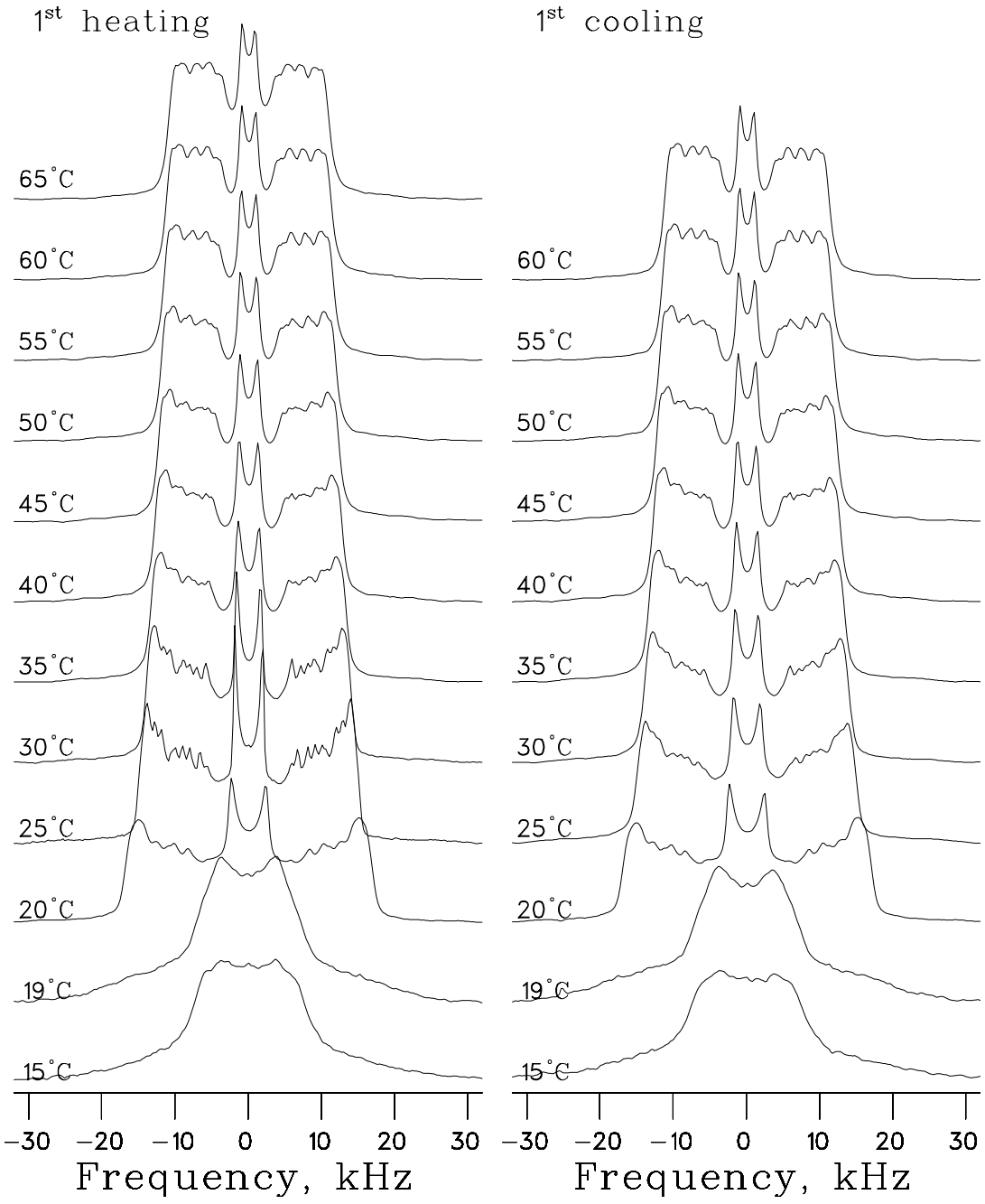

Figure 4.1: Powder spectra of d_{54}-DMPC sample at various temperatures

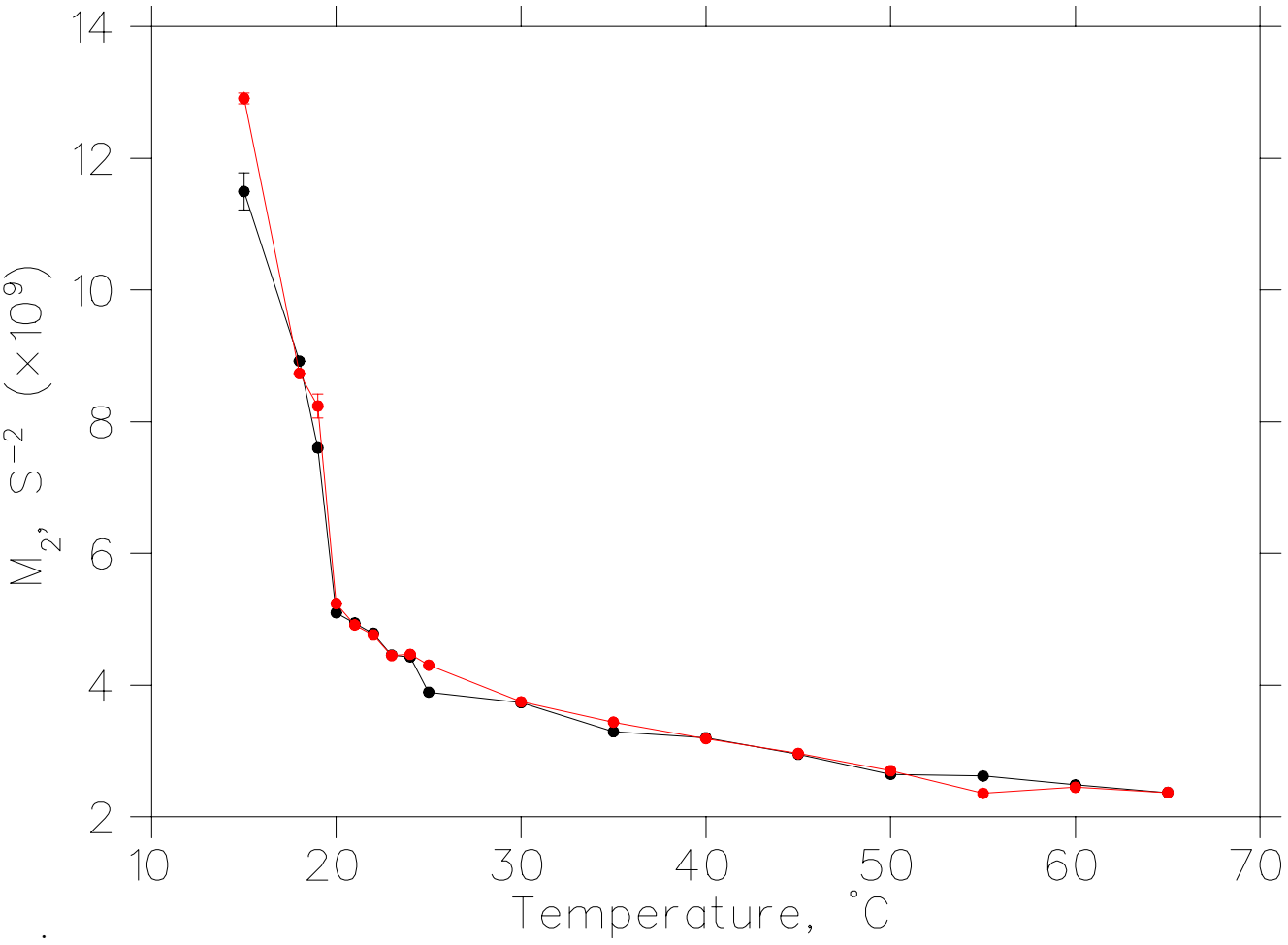

Figure 4.2: Temperature dependence of the second moments of the d_{54}-DMPC spectra from Fig. 4.1 through a heating then cooling run of the sample. The black line represents the "first heating" while the red line represents the "first cooling" cycle started from the last heating temperature 65°C. The error bars shown represent the standard deviations of the average M_2 values calculated by systematically varying the integration ranges in Eq. 3.1, well outside the spectral region (between ±85 kHz and ±100 kHz) for each spectrum in Fig. 4.1.

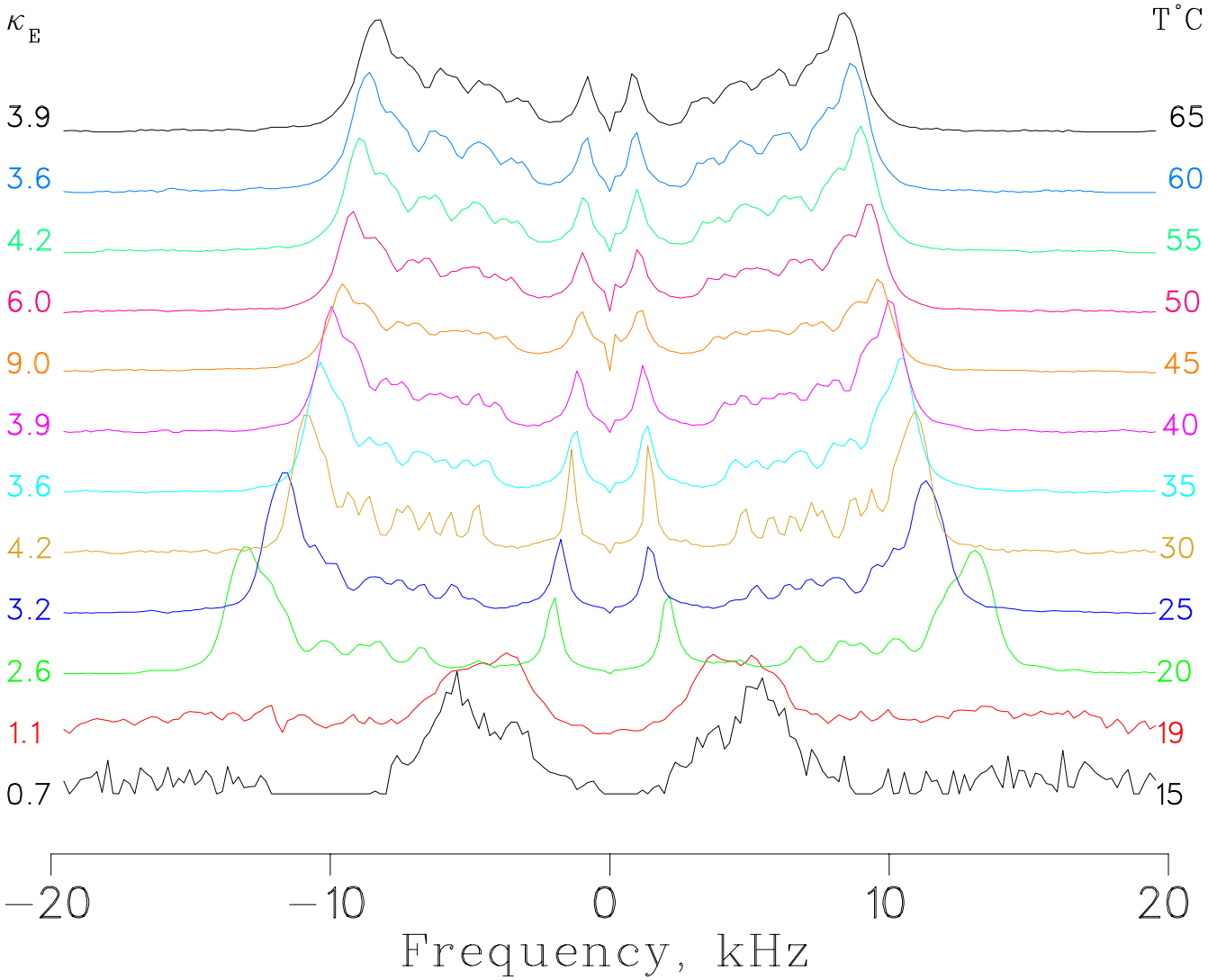

Figure 4.3: Normalized dePaked spectra of d_{54}-DMPC sample obtained at various heating temperatures. All the dePaked spectra were calculated using the ellipsoidal model at its minimum κ_E, as shown on the left.

long axis along the direction of the magnetic field, indicating the preferential alignment of the bilayers with their normal perpendicular to the magnetic field. The observed minima of the misfit functions were quite shallow in all cases above 20°C, and were quite sensitive to the noise in the spectra, so further quantitative conclusions cannot be made.

Assuming a monotonic decrease in the order parameter with the carbon position along the chain, a principle established by Seelig and Seelig [40], we can extract the order parameter profile by integrating the spectral intensity and dividing it in 2-2-2...-2-3 ratios as appropriate for a saturated carbon chain $(CH_2)_{12}$–CH_3 of the DMPC, even when the individual peak positions cannot be assigned. This is the so-called "average order parameter" approximation [8]. This is shown in Fig. 4.4. The order parameter profiles at lower temperatures exhibit the characteristic plateau shape for the carbon 2-8 positions, while at higher temperatures the order profiles exhibit a slightly more rapid decrease of the motional order towards the end of the chains.

4.2 10:1 and 3:1 DMPC:CHX samples, thermal hysteresis

When chlorhexidine is added to the DMPC membrane, the situation changes significantly. Figure 4.5 demonstrates significant differences between the spectra taken at the same temperatures within the heating and cooling cycles. This is made apparent by the temperature dependence of the second moment, shown in Fig. 4.6. There is a strong suggestion that the first time the sample temperature is raised above T_m after a long equilibration at low temperature, a sample undergoes an irreversible change.

Unfortunately, this was detected too late and the second heating/cooling cycles were not performed before the sample deteriorated.

The corresponding results for the 3:1 d_{54}-DMPC:CHX sample are presented in Figs. 4.7 and 4.8, through two heating/cooling cycles: equilibrate at 4°C; 12°C heating to 70°C, then cooling to 35°; equilibrate at 4°C overnight; 12°C heating to 60°C, then cooling to 15°C. As seen in the spectra of Figs. 4.7–4.8 (not all temperatures are shown for clarity) the spectra of the first cooling and second heating and cooling cycles are quite similar, with the first heating cycle being the only one significantly different from the other ones.

Fig. 4.9 confirms that through the temperature dependence of the second moments of the spectra for the four of the heating/cooling cycles. Because of the instrumental difficulties, the scatter of points is more pronounced, but the first heating cycle is clearly different from the other three which exhibit consistent second moment values in the 35°C–60°C range.

The anomalous zigzag behaviour at lower temperatures is probably an indication on non-equilibrium conditions in the sample. Again, this was only detected in subsequent analysis, and a longer equilibration time at each temperature was not attempted.

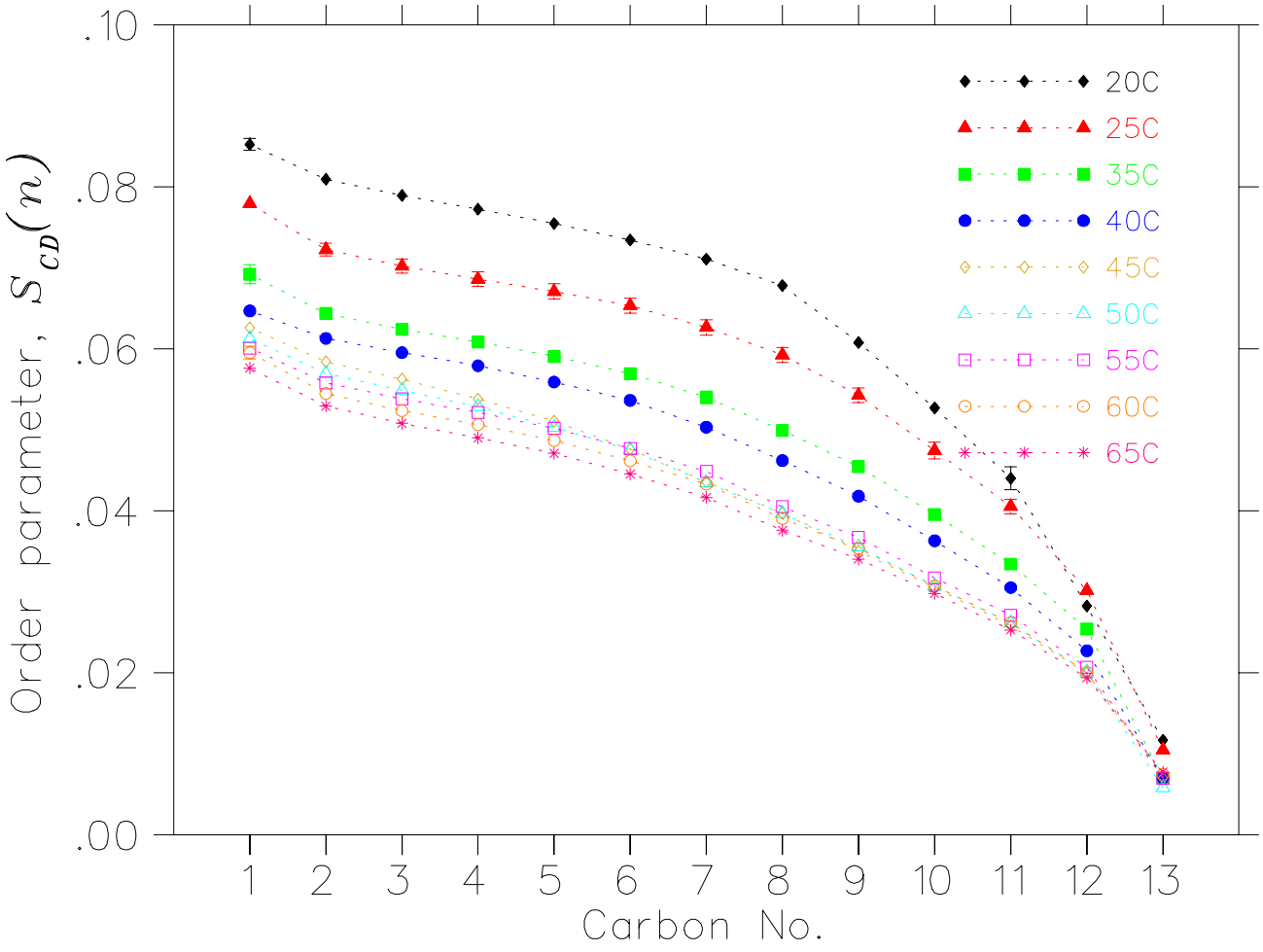

Figure 4.4: Order parameter profiles obtained from the dePaked spectra of the heating cycle of the d_{54}-DMPC sample. $n = 13$ carbon position corresponds to the CH_3 group of each spectrum. The rest of carbon positions represent the rest of CH_2 groups of the lipid molecules. The individual CH_2 splittings were not assigned; instead the average order parameters were calculated by dividing the integral intensity into 12 equal fractions.

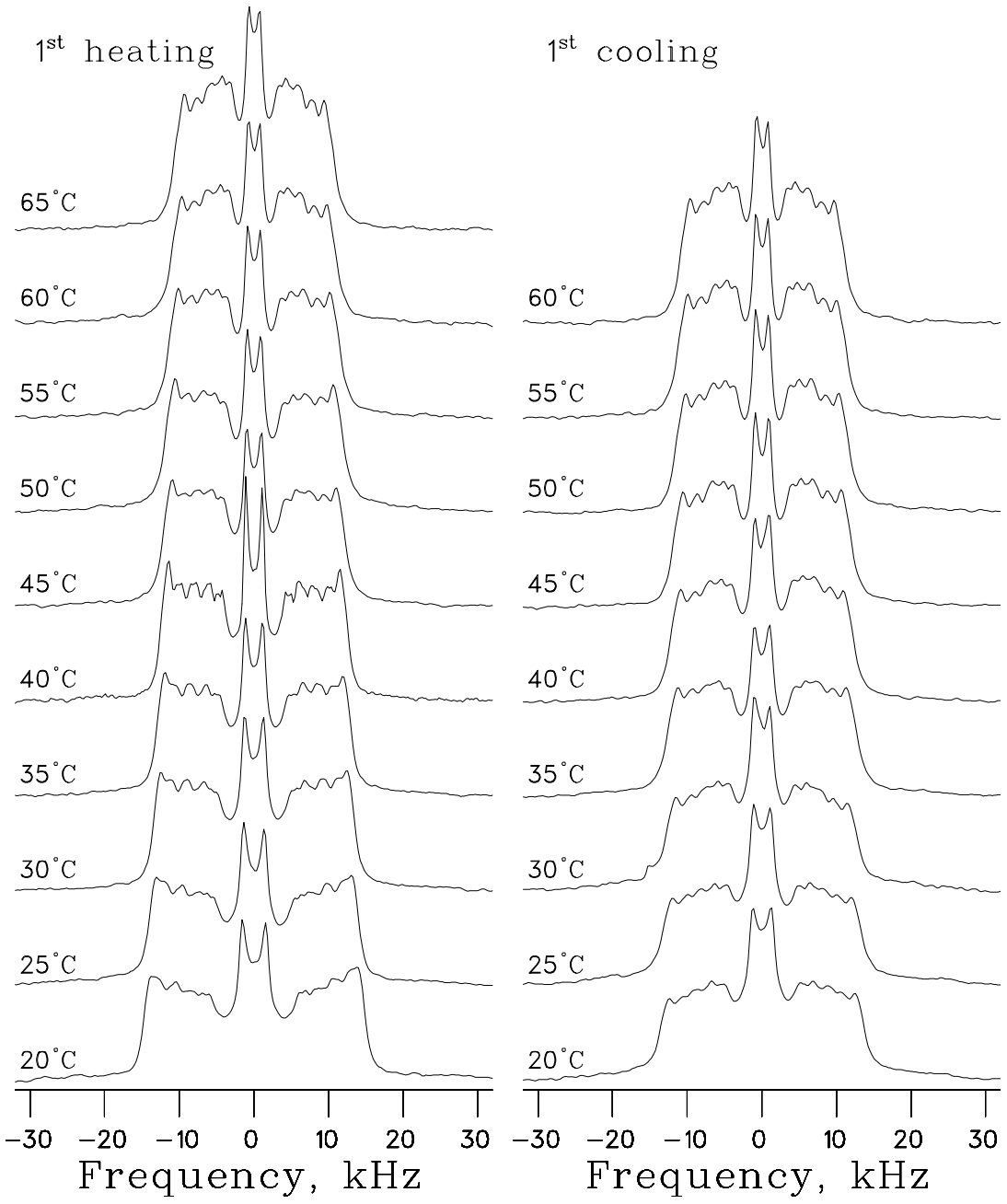

Figure 4.5: Spectra of 10:1 d_{54}-DMPC:CHX sample, "first heating" followed by the "first cooling" cycles. The spectra of the first cycle differ from the spectra of the second cycle from 20° to 50°

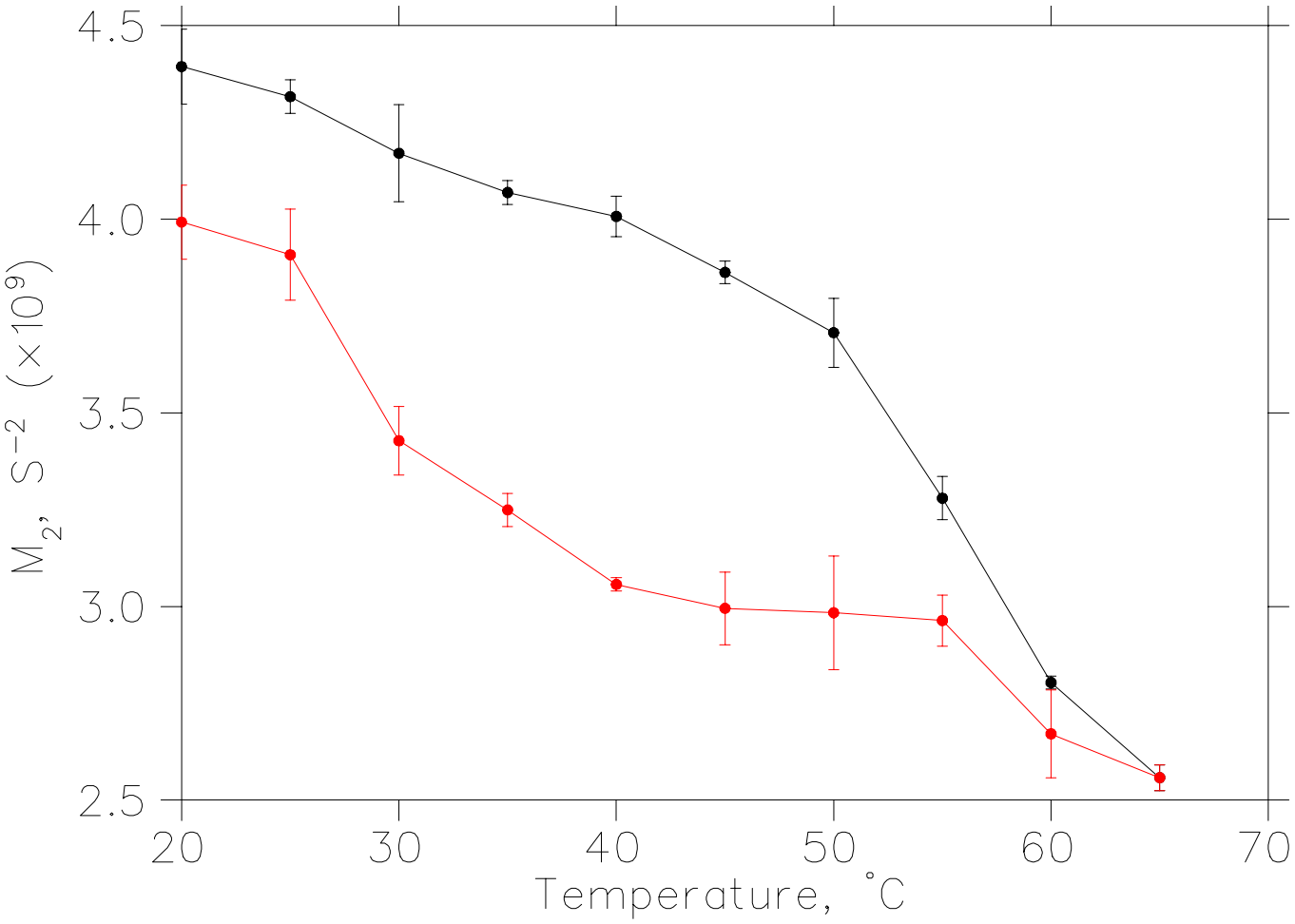

Figure 4.6: Temperature dependence of the second moments of the spectra of 10:1 d_{54}-DMPC:CHX sample through first heating (black line) then first cooling (red line) cycles. The error bars shown here were calculated in the same way discussed in the previous M_2 plot

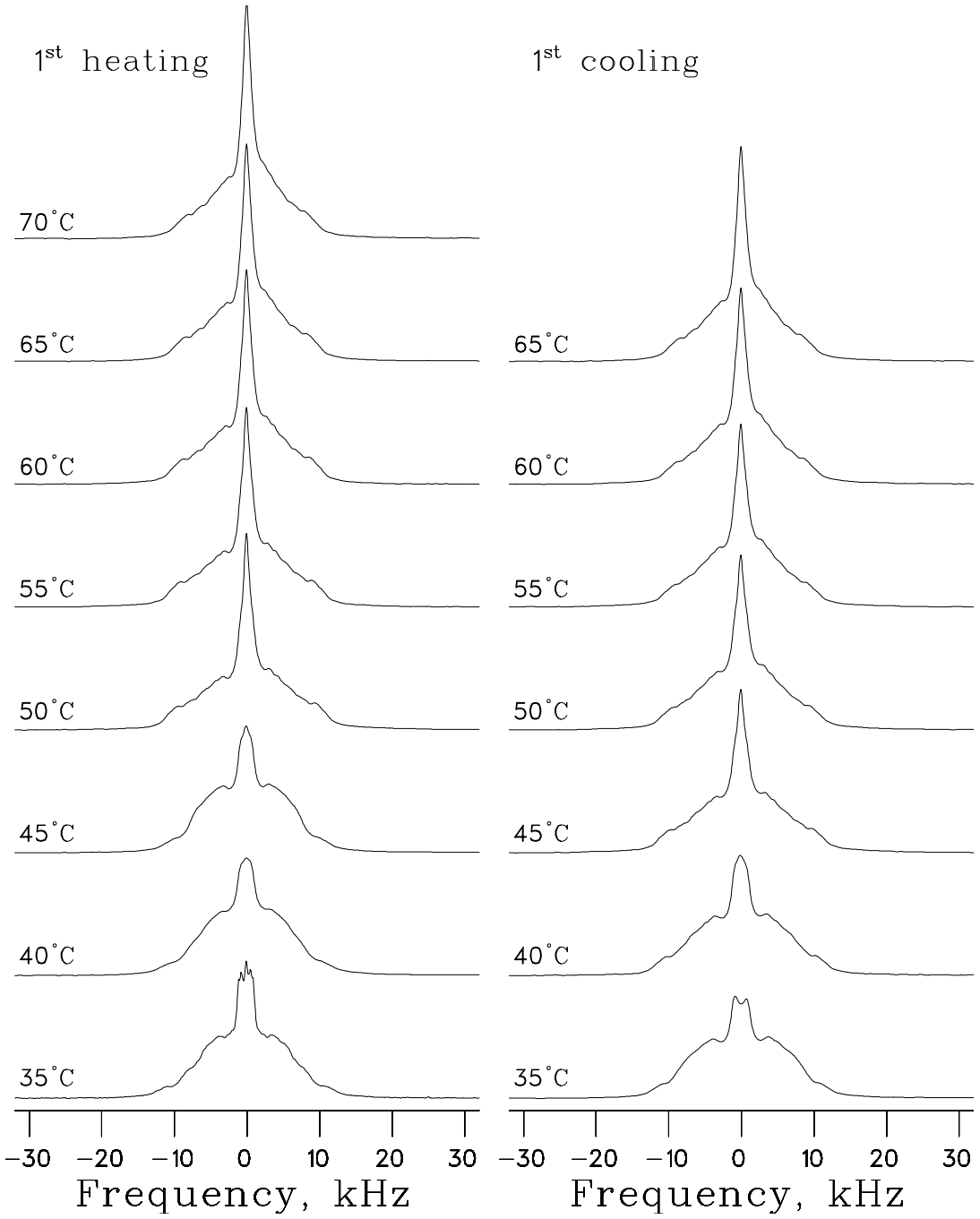

Figure 4.7: The spectra of 3:1 d_{54}-DMPC:CHX sample of the first heating/cooling cycle. The spectra of the first heating run are quite different than the ones of the first cooling specifically at temperatures 35°–55°C.

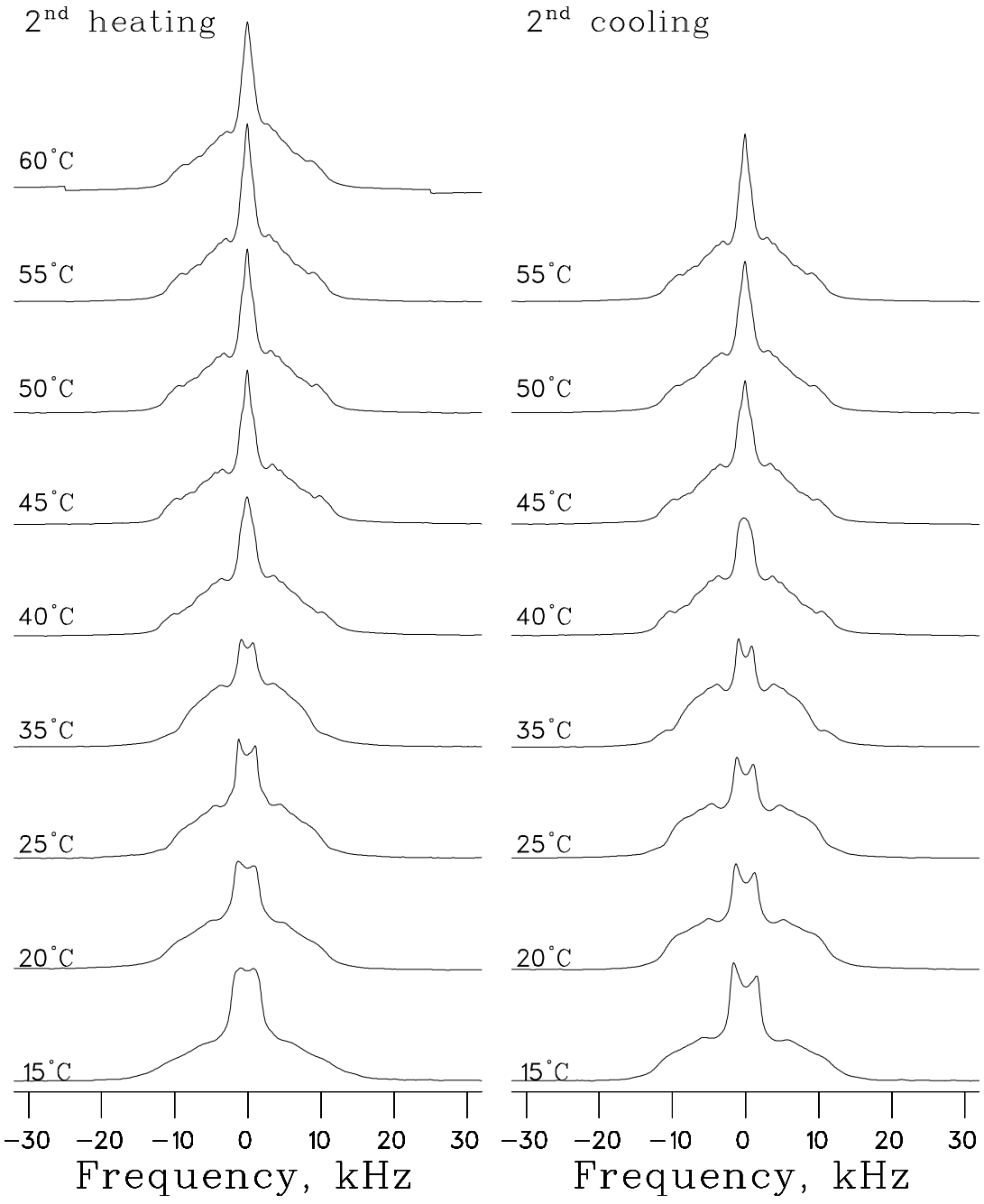

Figure 4.8: The spectra of 3:1 d_{54}-DMPC:CHX sample of the second heating/cooling cycle. Starting from 35°C, the spectra are highly similar to each other and to the ones in the first cooling cycle (see Fig. 4.7)

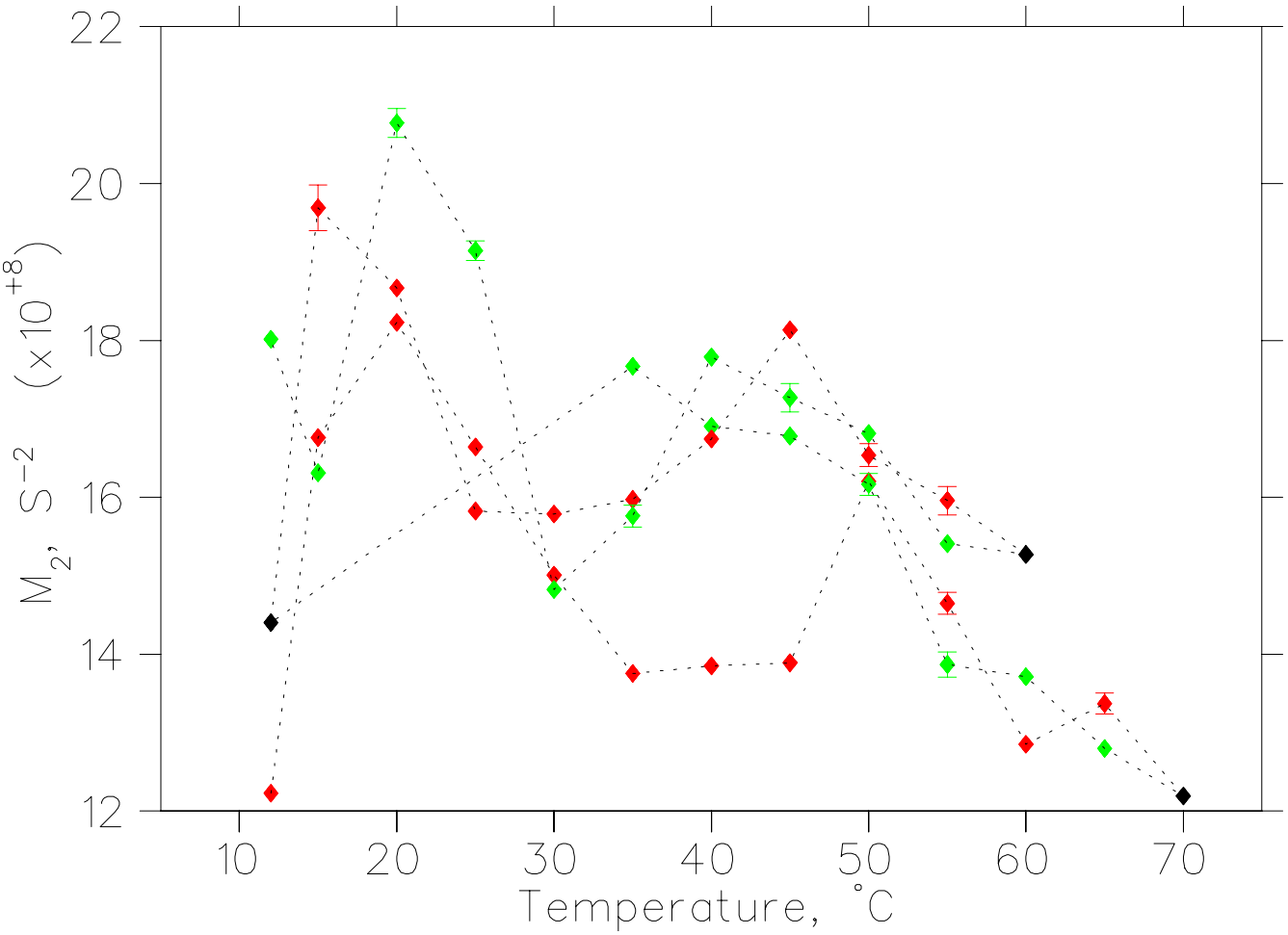

Figure 4.9: The second moments of the 3:1 d_{54}-DMPC:CHX spectra as a function of temperatures through two heating/cooling cycles. The two dotted lines with red diamonds represent the first and second heating cycles while the two dotted lines with green diamonds represent the cooling cycles. The black diamonds indicate to the temperatures at which a new cycle starts. For example, the first heating cycle starts at 12°C with a red diamond to extend all the way to the black diamond at 70°C where the first cooling cycle begins and follows along with the green diamonds to reach 35°C. The error bars shown here were calculated in the same way discussed in the first M_2 plot

4.3 10:1 and 3:1 DMPC:CHX samples, order parameters

In view of the results of the previous section, only the spectra obtained after the first heating cycle and a subsequent cooling were used for further analysis, for both 10:1 and 3:1 d_{54}-DMPC:CHX samples. The results of dePakeing are shown in Figs. 4.10 and 4.11. Both the spectral shapes and the minimal value of κ_E required to achieve convergence have a clearly anomalous value in the 25°C–35°C range. This clearly requires a more careful investigation at both CHX concentrations.

The corresponding average order parameter profiles are shown in Figs. 4.12 and 4.13. Compared to the pure DMPC case, the average order parameters decrease almost linearly with the carbon number, in a manner similar to that observed in the hexagonal H_{II} phase spectra [8]. This is true at both CHX concentrations. In addition, the temperature dependence may be indicative of a narrow re-entrant region in the 25°C–35°C range with a dramatic jump in the shape and the scale of the order parameter profile. In general, order parameters tend to show only very small and subtle changes and the observed temperature-dependent anomaly is quite startling. If confirmed in a repeated experiment, it may indicate a structural phase transition in this range of temperatures.

Other features of both order parameter profiles are quite typical of model membranes: the overall scaling trend with temperature, and the clearly different scaling for the terminal methyl group.

4.4 10:1 DMPC:CHX-d_8 sample

A counterpart to the 10:1 d_{54}-DMPC:CHX sample, the 10:1 DMPC:CHX-d_8 sample allows a comparison of the order parameters of the deuterated CH_2 groups on the hexamethylene bridge of CHX. There are only two inequivalent positions on the chain, and so the ^{2}H NMR spectra are much simpler, with only two non-overlapping doublets. The signal-to-noise is greatly reduced but an unambiguous assignment can still be made.

Fig. 4.14 shows the spectra of the 10:1 DMPC:CHX-d_8 sample. There is no evidence of thermal hysteresis, but for consistency, the cooling-cycle spectra were used in subsequent analysis. Because of the simplicity of the spectral structure, the dePaked spectra at each temperature were simply fitted to two Gaussian doublets. Representative examples at 25°C and 35°C are shown in Figs. 4.15 and 4.16, where the corresponding quadrupolar splittings are obtained as the values of best fit to two Gaussian doublets. These results are summarized in Table 4.1. There is no noticeable temperature dependence to the quadrupolar splittings.

Although no direct comparison is possible of the order parameters between the two molecular environments that are so vastly different, it is instructive to summarize the results in a single figure, for those temperatures where both sets of data exist (deuterated lipids, protonated CHX, and protonated lipids, deuterated CHX, at 10:1 molar ratio). This is done in Fig. 4.17. The apparent lack of temperature dependence is in stark contrast to the significant changes in the order parameter profiles of the lipids. This is consistent with the CHX methylene bridge being located in a highly mobile (despite the

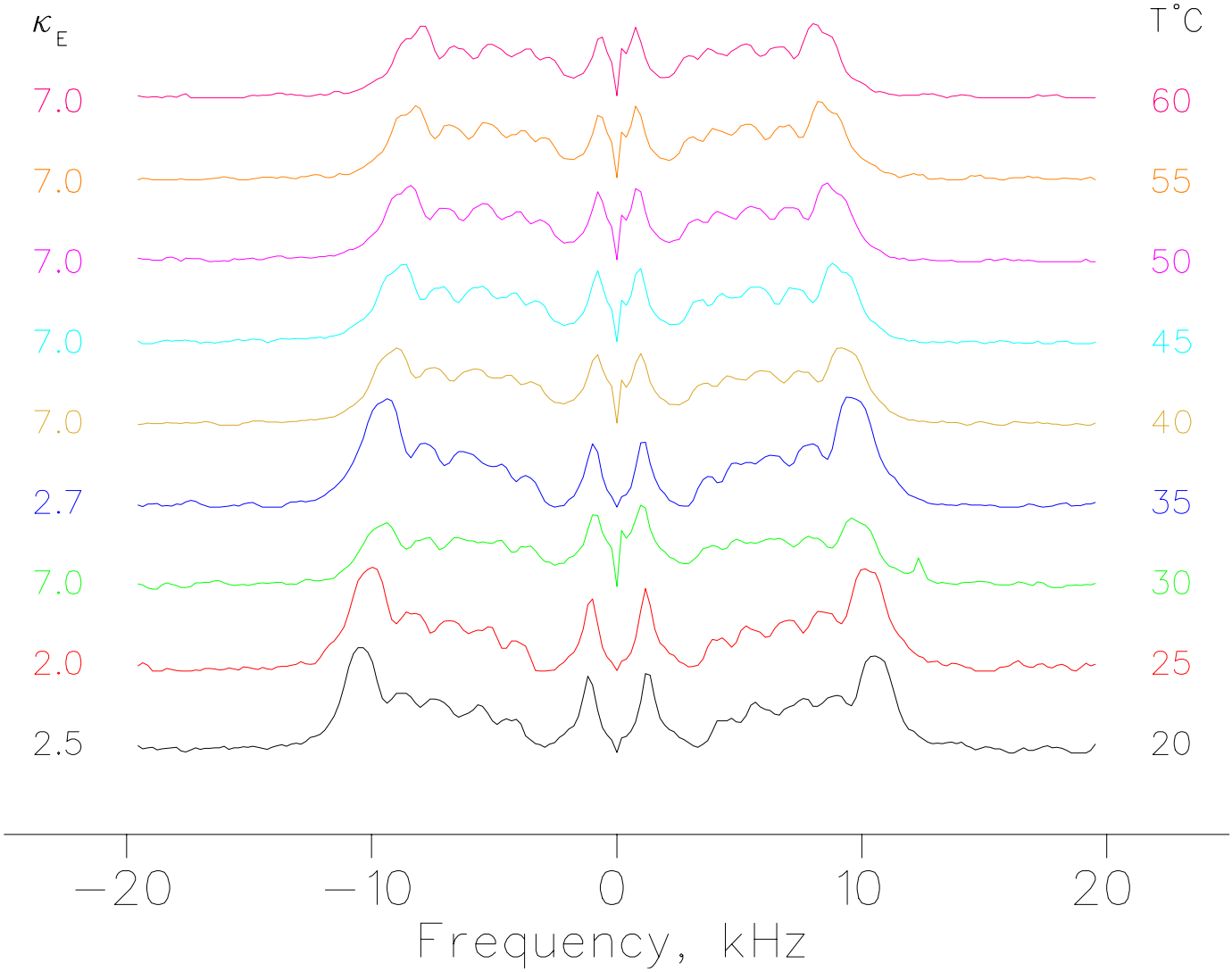

Figure 4.10: The dePaked spectra of the d_{54}-DMPC:CHX sample at 10:1 concentration obtained from the spectra of the cooling cycle. All the dePaked spectra have been performed using the ellipsoidal model at their lowest minima κ_E shown on the left.

Table 4.1: Quadrupolar splittings obtained from the dePaked spectra of the 10:1 DMPC:CHX-d_8 sample

Temperature, °C	$\Delta\omega_q^{(1)}$	$\Delta\omega_q^{(2)}$
55	1.41 ± 0.01	0.92 ± 0.01
45	1.48 ± 0.01	0.91 ± 0.01
35	1.48 ± 0.01	0.91 ± 0.01
25	1.47 ± 0.01	0.90 ± 0.01

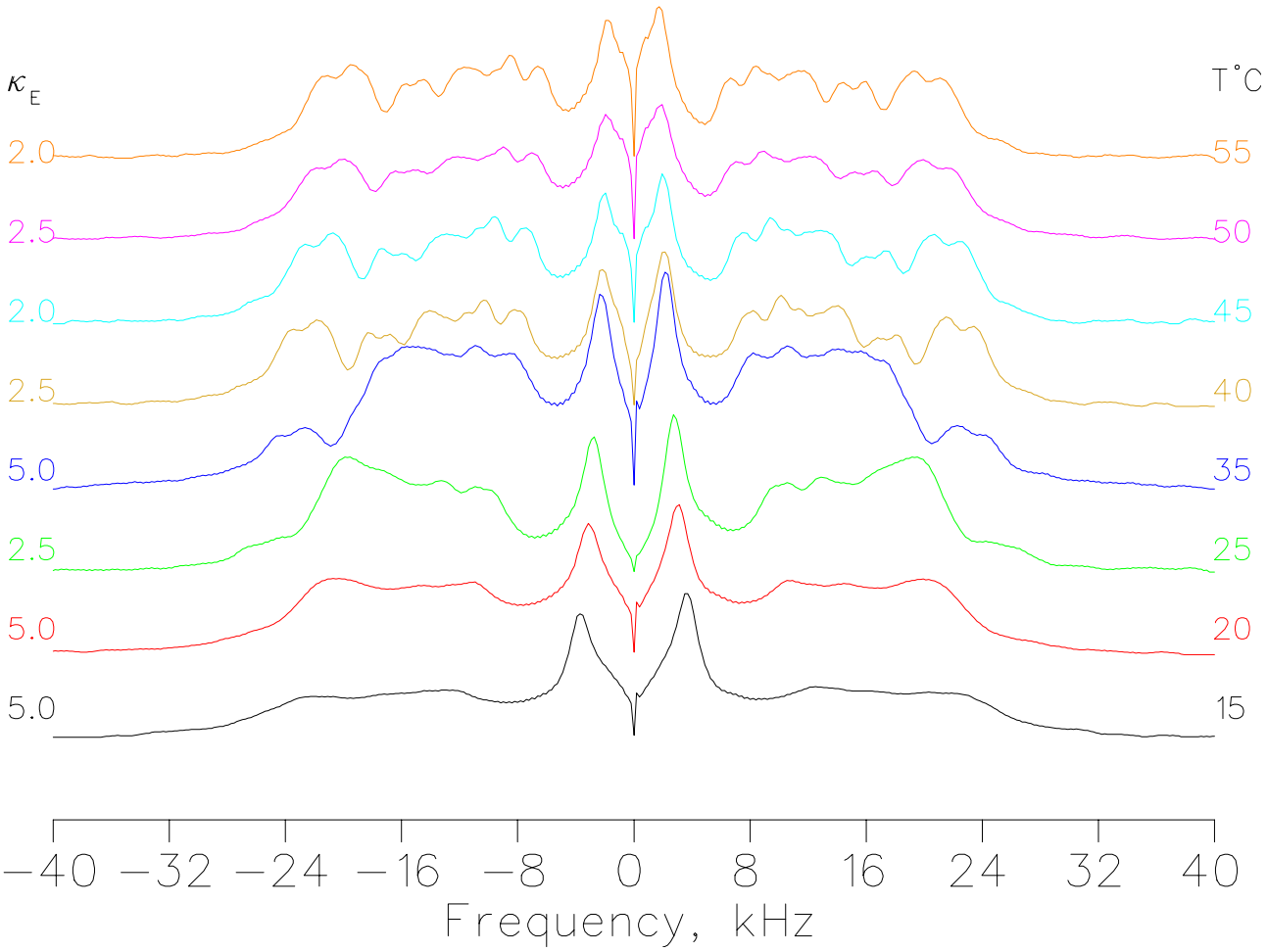

Figure 4.11: The dePaked spectra of 3:1 d_{54}-DMPC:CHX sample at various temperatures. The minimum of each spectrum illustrated by κ_E is on the left side of each spectrum.

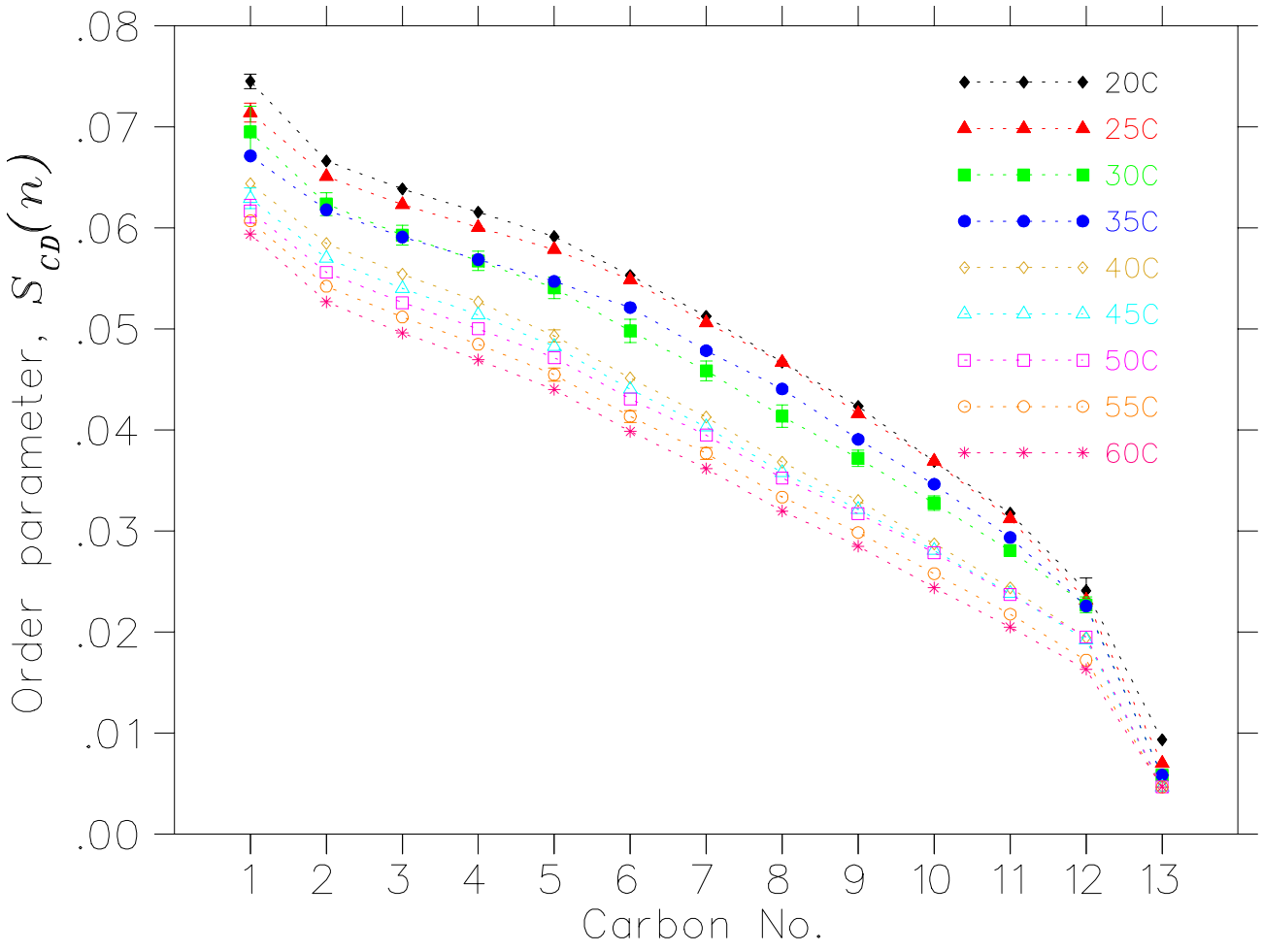

Figure 4.12: Order parameter profiles of the 10:1 d_{54}-DMPC:CHX sample as extracted from the dePaked spectra of Fig. 4.10

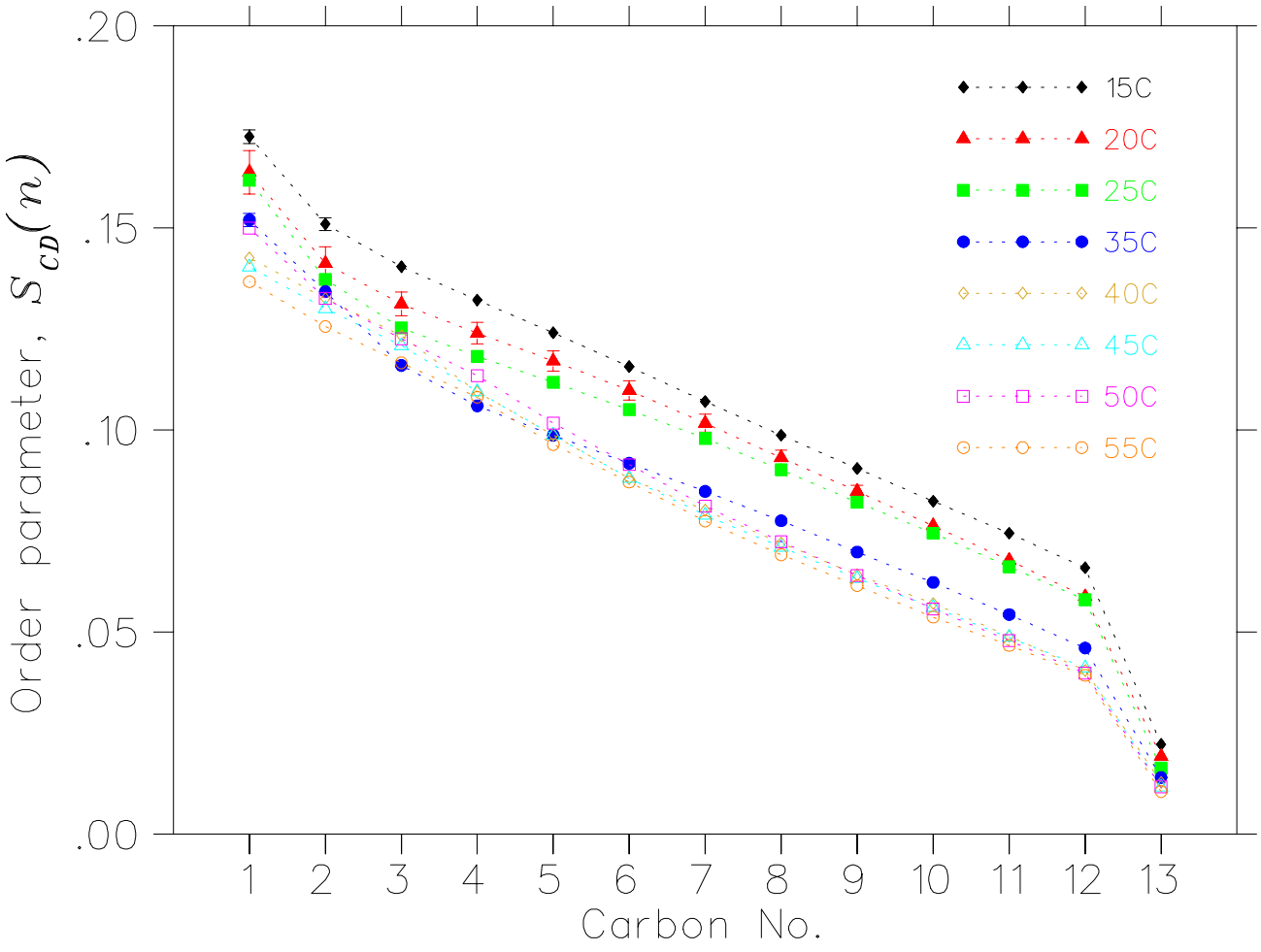

Figure 4.13: Order parameter profiles of 3:1 d_{54}-DMPC:CHX sample, as extracted from the dePaked spectra of Fig. 4.11

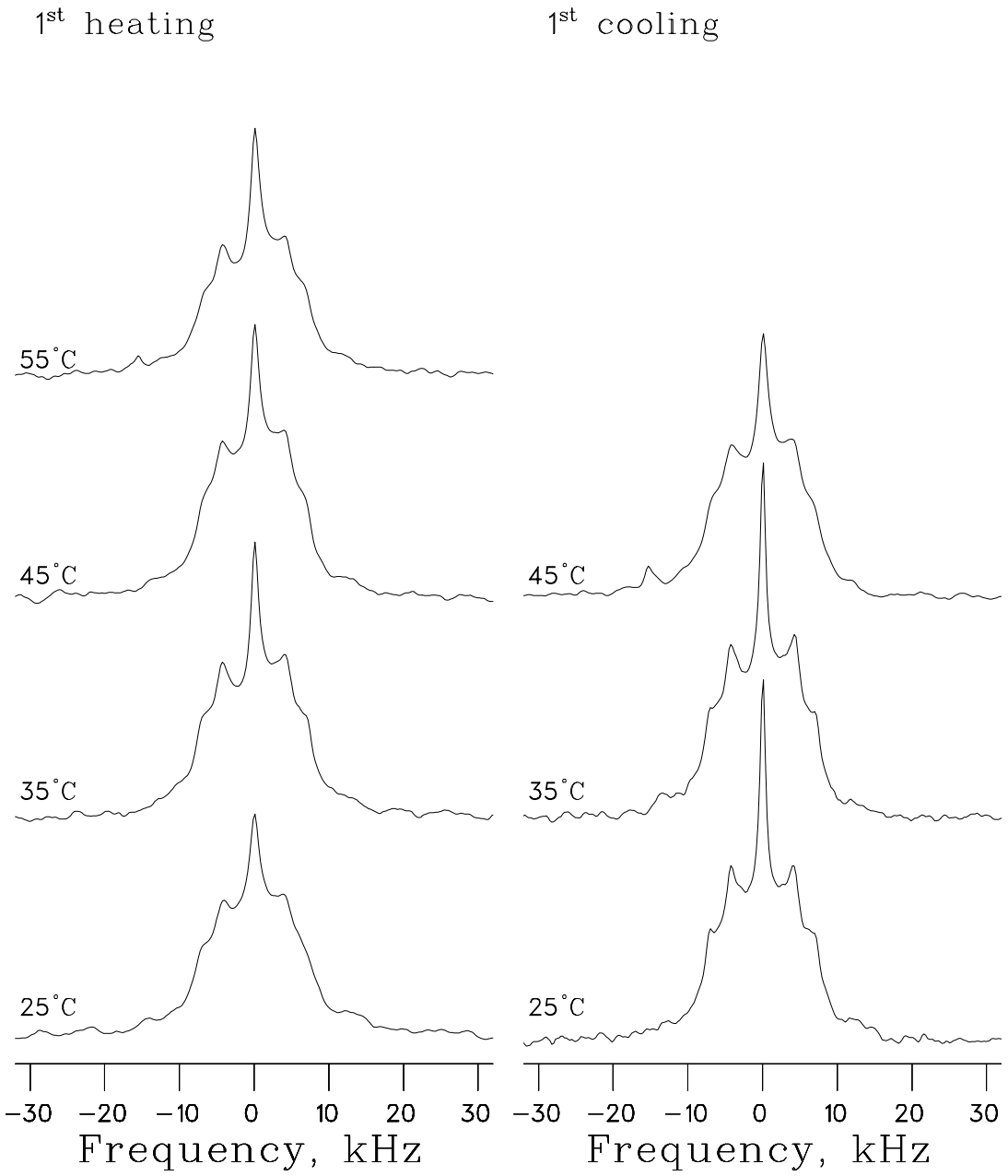

Figure 4.14: 10:1 DMPC:CHX-d_8 spectra

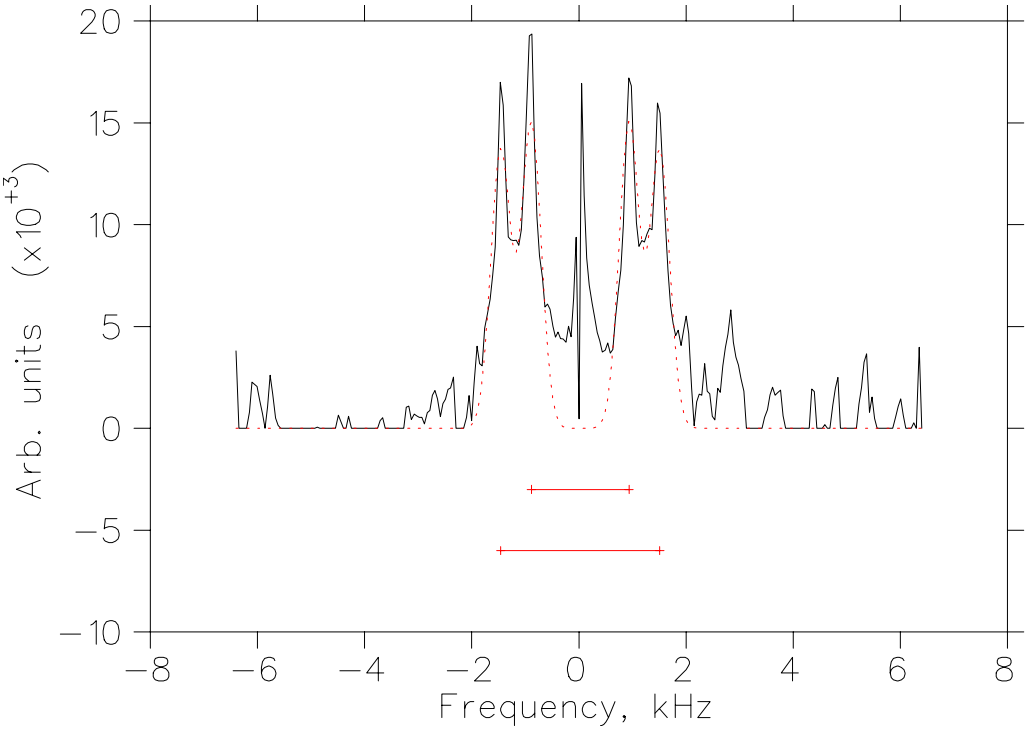

Figure 4.15: The dePaked spectrum of the 10:1 DMPC:CHX-d_8 sample at 35°C with the refined first and second quadrupolar splittings (two Gaussian doublets). The line of best fit is shown in red. The results of the fit are: $\Delta\omega_q^{(1)} = 0.91 \pm 0.01$ and the second is $\Delta\omega_q^{(2)} = 1.48 \pm 0.01$

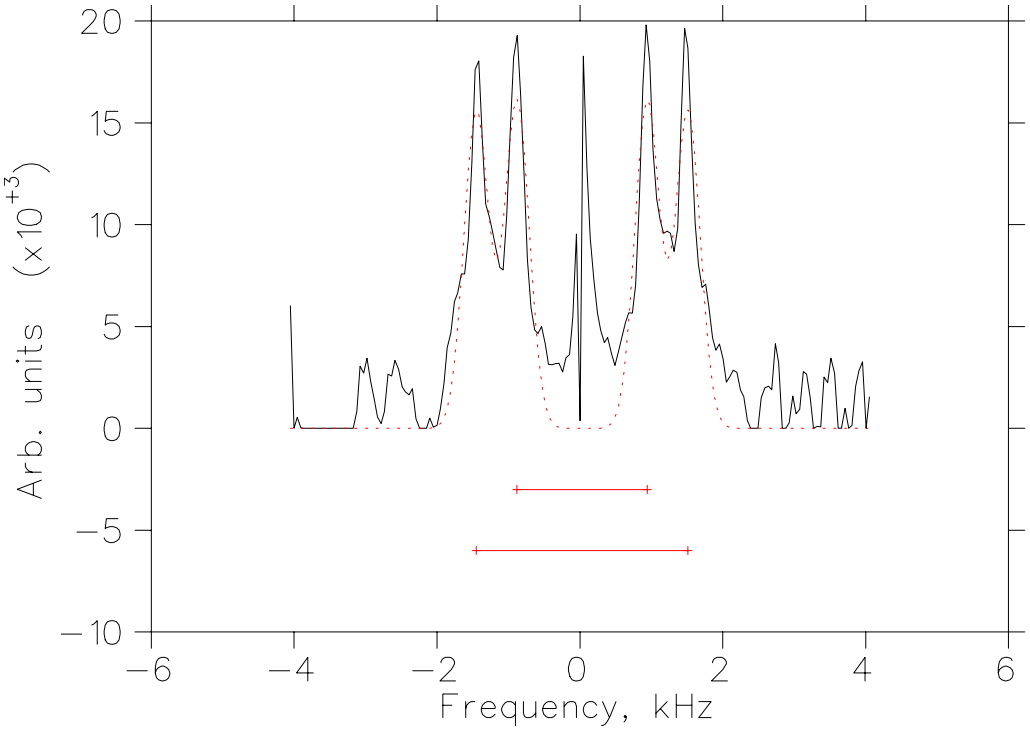

Figure 4.16: The dePaked spectrum of the 10:1 DMPC:CHX-d_8 sample at 25°C with the refined first and second quadrupolar splittings (two Gaussian doublets). The line of best fit is shown in red. The results of the fit are: $\Delta\omega_q^{(1)} = 0.90 \pm 0.01$ and the second is $\Delta\omega_q^{(2)} = 1.47 \pm 0.01$

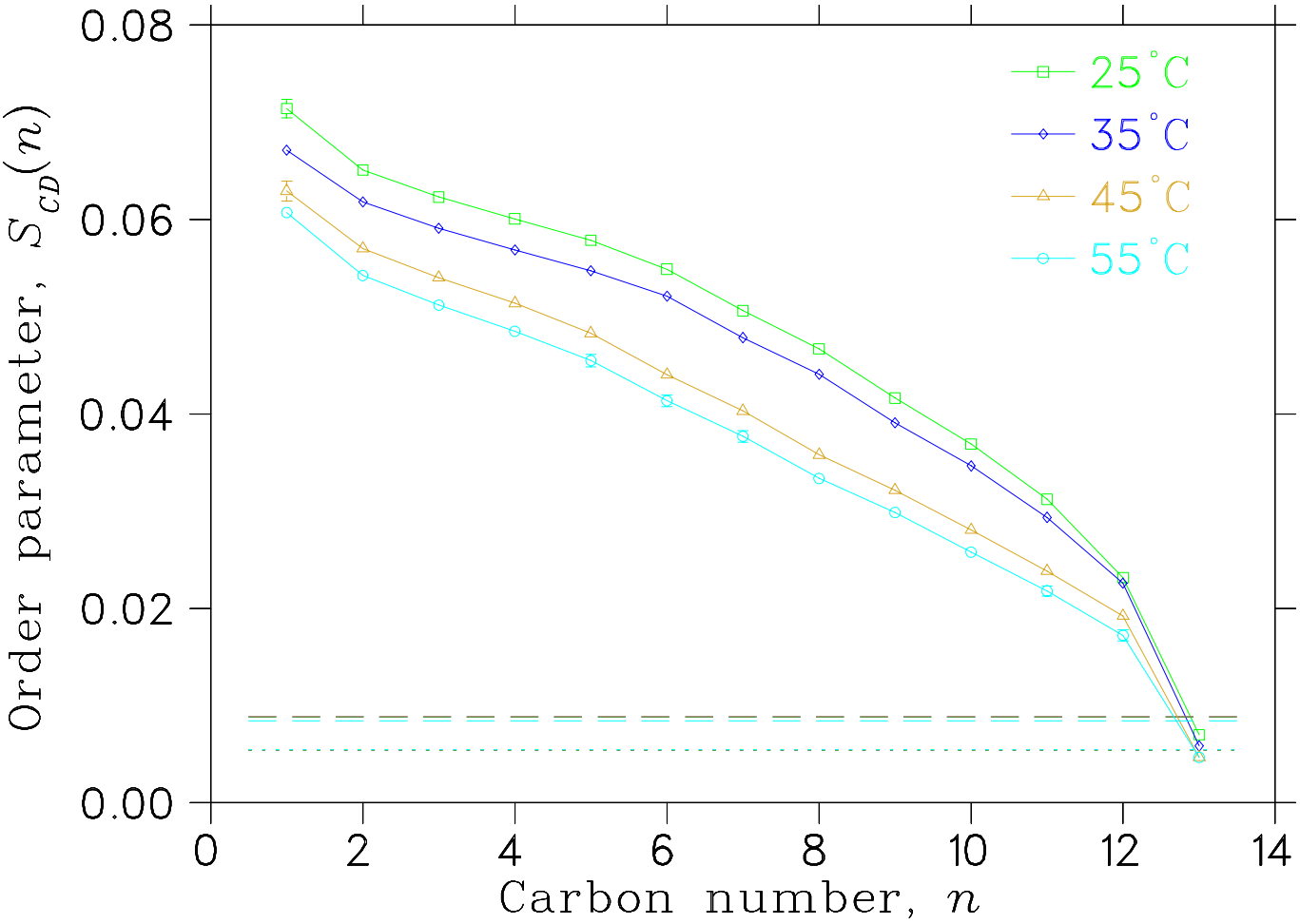

Figure 4.17: Order parameter profiles of the 10:1 d_{54}-DMPC:CHX sample at select temperatures compared to those of the 10:1 DMPC:CHX-d_8 sample at the same temperatures. The temperatures are taken starting from the last heating temperature 55°C to the following cooling temperatures 45°C, 35°C, then 25°C. The dotted lines represent the values of $\Delta\omega_q^{(1)}$ and the dashed lines represent $\Delta\omega_q^{(2)}$. The values, and the horizontal lines are indistinguishable for all temperatures.

two aromatic "anchors" at both ends) environment that is not greatly affected by the thermal changes taking place in the bulk of the lipid bilayer. This is suggestive of the CHX molecules experiencing an environment other than the bulk lipids, in agreement with the neutron scattering data of Komljenovic *et al.*

Chapter 5

Conclusions

The extensive data re-analysis to address the issues of thermal hysteresis and potentially significant numerical errors prevented the completion of the additional measurements of the small amounts remaining of deuterated CHX, a unique compound not available commercially. Nevertheless, a thorough investigation of all of the previously acquired data was performed, including the examination and verification of previously used experimental protocols, and a careful re-processing of all spectra previously acquired.

Based on the result of the newly re-analyzed data, it is evident that the ^{2}H NMR data is consistent with the neutron scattering data obtained previously for the same system. The comparison of temperature dependence of the order parameters of CH_2 groups on the fatty acid chains of the lipids (strong, and consistent with pure lipid data) and on chlorhexidine (no observable temperature dependence) indicates that the CHX molecule is not undergoing the same kind of motions as the bulk lipids in the membrane. This is again consistent with the neutron scattering and the molecular modeling data.

A potentially anomalous phase behavior was detected in the same range of temperatures for both concentrations of CHX in DMPC. It is tempting to attribute it to a new, re-entrant phase, but the quality of the data does not allow to draw such an unambiguous conclusion. More work needs to be done, in smaller temperature increments, using longer equilibration times at each temperature, and at additional concentrations of DMPC:CHX mixtures.

A potential weak point was identified in the protocol of sample preparation. It appears that the equilibration at an elevated temperature for more than a brief heating-up associated with freeze-thaw cycles used in sample mixing may be required for these samples.

Chapter 6

Appendix

Table 6.1 shows the summary of the origin of the data used in this work; the time-domain signals acquired by previous students were re-processed and re-analyzed from scratch.

Table 6.1: Data of the samples; 1:0 d_{54}-DMPC:CHX, 10:1 d_{54}-DMPC:CHX, 10:1 DMPC:CHX-d_8, 3:1 d_{54}-DMPC:CHX has been collected by previous students using ^{2}H NMR spectroscopy at Brock University

Samples	Temperatures, C°	Dates	References
1:0 d_{54}-DMPC	15...65...15	Sep 28–30, 2010	[1]
10:1 d_{54}-DMPC:CHX	20...65...20	Nov 5–7, 2010	[1]
10:1 DMPC:CHX-d_8	25...55...25	Nov 15, 2010	[1]
3:1 d_{54}-DMPC:CHX	12...70...12	Sep 28 – Oct 14, 2006	[23]

Bibliography

[1] I. Komljenovic, D. Marquardt, T. Harroun, and E. Sternin. Location of chlorhexidine in DMPC model membrane: A neutron diffraction study. *Europe PMC*, 163:480–487, 2010.

[2] B. van Oosten, D. Marquard, E. Sternin, and T.A. Harroun. Small molecule interaction with lipid bilayers: A molecular dynamics study of chlorhexidine. *Sci. Direc.*, 48:96–104, 2014.

[3] Philip L. Yeagle. *The Membranes of Cells*. Academic Press Inc., San Diego, USA, 1993.

[4] S.J. Singer and G.L. Nicholson. The fluid mosaic model of the structure of cell membranes. *Science*, 175:720–731, 1972.

[5] Mary Luckey. *Membrane Structural Biology With Biochemical and Biophysical Functions*. Cambridge University Press, New York, USA, 2nd edition, 2014.

[6] Christopher J. Fielding, editor. *Lipid Rafts and Caveolae from Membrane Biophysics to Cell Biology*. Wiley-Vch Verlag GmbH & Co. KGaA, Weinheim, Germany, 2006.

[7] T. G. Pomorskia, T. Nylander, and M.Cárdenas. Model cell membranes: Discerning lipid and protein contributions in shaping the cell. *Sci. Direc.*, 205:207–220, 2014.

[8] E. Sternin, B. Fine, M. Bloom, C.P. Tilcock, K.F. Wong, and P.R. Cullis. Acyl chain orientational order in the hexagonal H_{II} phase of phospholipid-water dispersions. *Biophysical Journal*, 54(4):689–694, 1988.

[9] R.B. Gennis. *Biomembranes Molecular Structure and Function*. Springer-Verlag, New York, NY 10032, USA, 1989.

[10] M. Eeman and M. Deleu. From biological membranes to biomimetic model membranes. *Base*, 14:719–736, 2010.

[11] How do lipid bilayer components move? URL `www.mechanobio.info/what-is-the-plasma-membrane/how-do-lipid-bilayer-components-move/`. Accessed: 2017/01/29.

[12] J. Katsaras and T. Gutberlet. *Lipid Bilayers Structure and Interactions*. Springer-Verlag, New York, USA, 2001.

[13] G. B. Schaefer and Jr. J. N. Thompson. *Medical Genetics: An Integrated Approach*. McGraw-Hill Education, New York, 2014. URL `http://accessmedicine.mhmedical.com/content.aspx?bookid=2247`. Chapter 13: Disorders of organelles. Accessed March 05, 2018.

[14] Chlorhexidine. URL `https://en.wikipedia.org/wiki/Chlorhexidine`. Accessed: 2017/01/29.

[15] About chlorhexidine: Mechanism of action. URL `http://chlorhexidine-facts.com/mechanismof-action.html`. Accessed: 2017/04/13.

[16] W.B. Hugo and A.R. Longworth. Some aspects of the mode of action of chlorhexidine. *J. Pharm. Pharmacol.*, 16:655–662, 1964.

[17] M.A. Altannir and H.S. Goodman. A review of chlorhexidine and its use in special populations. *Special Care in Dentistry*, 14:116—-122, 1994.

[18] K. Barrett-Bee, L. Newboult, and S. Edwards. The membrane destabilising action of the antibacterial agent chlorhexidine. *FEMS Microbiol. Lett.*, 119:249–254, 1994.

[19] W. Kunkitti, D. Lloyed, J.R.Furr, and A.D. Russel. Aspects of the mechanism of action of biguanides on trophozoites and cysts of acanthamoeba castellanii. *J. of Applied Microbiology.*, 82:107–114, 1997.

[20] G. Kaur, A. Singh, K. P. Patil, ?. Gopalakrishnan, A. S. Nayyar, and S. Deshmukh. Chlorohexidine: A cationic bisbiguanide, membrane active drug in periodontal medicine, structure, advantages and associated adverse effects, a brief communication. *W. J. of Pharm. and Pharmaceut. Sci.*, 4:370–392, 2015.

[21] I. Komljenovic. *Elucidation of a Mechanism of Cell Lysis by Chlorhexidine: A Biophysical Approach*. PhD thesis, Brock University, 2008.

[22] J.M. Tanzer, A.M. Slee, and B.A. Kamay. Structural requirements of guanide, biguanide, and bisbiguanide agents for antiplaque activity. *Antimicrob. Agents Chemother.*, 12:721–729, 1977.

[23] S. Sadeghi. Order and membrane organization in chlorhexidine-lipid mixture. Master's thesis, Brock University, 2006.

[24] Malcolm H. Levitt. *Spin dynamics, Basics of Nuclear Magnetic Resonance*. John Wiley and Sons, Ltd, Baffin Lane, Chichester, West Sussex PO19UD, England, 2001.

[25] C. Morrison. *Theory of the general orientation dependence of ^2H NMR spin-lattice relaxation and experiments on model membranes*. PhD thesis, University of British Columbia, 1993.

[26] J.H. Davis. The description of lipid membrane conformation, order, and dynamics by ^{2}H NMR. *Biochim. Biophys. Acta.*, 737:117–171, 1983.

[27] NMR of lipids. In Anthony Watts and G.C.K. Roberts, editors, *Encyclopedia of Biophysics*, Edinburgh, Scotland, 2013. European Biophysical Societies Association.

[28] Hartmut Schafer, Burkhard Madler, and Edward Sternin. Determination of Orientational Order Parameters from 2H NMR Spectra of Magnetically Partially Oriented Lipid Bilayers. *Biophys. J.*, 74(2):1007–1014, 1998.

[29] E. Sternin, M. Bloom, and A.L. Mackay. De-pake-ing of nmr spectra. *J. Magn. Reson.*, 55:274–282, 1983.

[30] G.E. Pake. Nuclear resonance absorption in hydrated crystals: Fine structure of the proton line. *J. Chem. Phys*, 16:327–336, 1948.

[31] J. H. Davis, K. R. Jeffrey, M. Bloom, M. I. Valic, and T. P. Higgs. *Quadrupolar Echo Deuteron Magnetic Resonance Spectroscopy in Ordered Hydrocarbon Chains*, chapter 7, pages 70–77.

[32] Edward Sternin, Myer Bloom, and Alexander L Mackay. De-Pake-ing of NMR spectra. *J. Magn. Reson.*, 55(2):274–282, 1983.

[33] E. Sternin, H. Schäfer, I.V. Polozov, and K. Gawrisch. Simultaneous determination of orientational and order parameter distributions from NMR spectra of partially oriented model membranes. *J. Magn. Reson.*, 149:110–113, 2001.

[34] H. Schäfer, B. Madler, and E. Sternin. Determination of orientational order parameters from ^{2}H NMR spectra of magnetically partially oriented lipid bilayers. *Biophys. J.*, 74:1007–1014, 1998.

[35] E. Sternin. Use of inverse theory algorithms in the analysis of biomembrane NMR data. In Alex M. Dopico, editor, *Methods in Membrane Lipids*, volume 400 of *Methods in Molecular Biology*, pages 103–125. Humana Press, 2007.

[36] M. Moser, T. Hudlicky, S. Sadeghi, and E. Sternin. Synthesis of deuterium labelled chlorhexidine. *J. Label. Compd. Radiopharm.*, 50:671–674, 2007.

[37] E. Sternin. Radio frequency phase shifting at the source simplifies NMR spectrometer design. *Rev. Sci. Instrum.*, 66:3144–3145, 1995.

[38] A.A. Bele and A.Khale. An overview on thin layer chromotography. *I. J. of Pharmaceut. Sci. and Res.*, 2:256–267, 2011.

[39] F. Vitiello and J.P. Zanetta. Thin-layer chromatography of phospholipids. *J. of Chromatography*, 166:637–640, 1978.

[40] J. Seelig and A. Seelig. Lipid conformation in model membranes and biological membranes. *Q. Rev. Biophys.*, 13:19–61, 1980.